

AD-770 074

SCALING GENERALIZATIONS FOR A PULSED
CO EDL (ELECTRIC DISCHARGE LASER)

W. B. Lacina

Northrop Research and Technology Center

Prepared for:

Office of Naval Research

October 1973

DISTRIBUTED BY:

NTIS

National Technical Information Service
U. S. DEPARTMENT OF COMMERCE
5285 Port Royal Road, Springfield Va. 22151

AD 720074



DDC
RECEIVED
NOV 6 1973
B

DISTRIBUTION STATEMENT A
Approved for public release
Distribution Unlimited

NORTHROP

Research and Technology Center

AD-770074

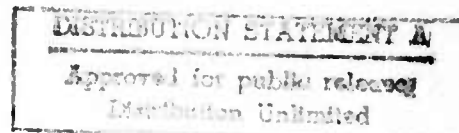
SCALING GENERALIZATIONS FOR A
PULSED CO EDL

October 1973



Prepared by

W. B. Lacina



Contract No. N00014-72-C-Q043

Sponsored by
ADVANCED RESEARCH PROJECTS AGENCY
ARPA ORDER No. 1806


Monitored by
OFFICE OF NAVAL RESEARCH
CODE 421

Northrop Research and Technology Center
3401 West Broadway
Hawthorne, California 90250

Reproduced by
NATIONAL TECHNICAL
INFORMATION SERVICE
U S Department of Commerce
Springfield VA 22151

UNCLASSIFIED

SECURITY CLASSIFICATION OF THIS PAGE (When Data Entered)

REPORT DOCUMENTATION PAGE		READ INSTRUCTIONS BEFORE COMPLETING FORM
1. REPORT NUMBER NRTC 73-43R	2. GOVT ACCESSION NO.	3. RECIPIENT'S CATALOG NUMBER
4. TITLE (and Subtitle) Scaling Generalizations for a Pulsed CO EDL		5. TYPE OF REPORT & PERIOD COVERED Technical Report
7. AUTHOR(s) W. B. Lacina		6. PERFORMING ORG. REPORT NUMBER
9. PERFORMING ORGANIZATION NAME AND ADDRESS Northrop Research and Technology Center 3401 West Broadway Hawthorne, California 90250		8. CONTRACT OR GRANT NUMBER(s) N00014-72-C-0043
11. CONTROLLING OFFICE NAME AND ADDRESS Advanced Research Projects Agency 1400 Wilson Blvd Arlington, Virginia 22209		10. PROGRAM ELEMENT, PROJECT, TASK AREA & WORK UNIT NUMBERS ARPA Order No. 1806
14. MONITORING AGENCY NAME & ADDRESS (if different from Controlling Office) Office of Naval Research Department of the Navy Arlington, Virginia 22217		12. REPORT DATE October 1973
		13. NUMBER OF PAGES 45
		15. SECURITY CLASS. (of this report) Unclassified
16. DISTRIBUTION STATEMENT (of this Report) 		15a. DECLASSIFICATION/DOWNGRADING SCHEDULE
17. DISTRIBUTION STATEMENT (of the abstract entered in Block 20, if different from Report) None.		
18. SUPPLEMENTARY NOTES None.		
19. KEY WORDS (Continue on reverse side if necessary and identify by block number) CO Laser Electric Discharge Scaling Generalizations Saturation Intensity Quantum Efficiency Molecular Kinetics Oscillator Analysis Transient Analysis		
20. ABSTRACT (Continue on reverse side if necessary and identify by block number) Several scaling generalizations for apulsed CO EDL are presented and discussed. Quantum efficiency is shown to be mainly dependent upon total energy deposition as a function of time. Typically, turn-on occurs after ~1 J/liter/torr has been deposited, and steady state after ~2 J/liter/torr. Scaled saturation intensity is ~0.6 - 6.0 W/cm ² /torr ² .		

DD FORM 1 JAN 73 1473

EDITION OF 1 NOV 65 IS OBSOLETE

UNCLASSIFIED

SECURITY CLASSIFICATION OF THIS PAGE (When Data Entered)

NOTICE

The views and conclusions contained in this document are those of the author and should not be interpreted as necessarily representing the official policies, either expressed or implied, of the Advanced Research Projects Agency or the U. S. Government.

TABLE OF CONTENTS

ABSTRACT	1
1.0 INTRODUCTION	2
2.0 MOLECULAR KINETIC MODEL: SUMMARY	4
3.0 APPROXIMATIONS AND SCALING GENERALIZATIONS	11
4.0 DISCUSSION AND NUMERICAL RESULTS	15
FIGURES	21-44
REFERENCES	45

ABSTRACT

Several scaling generalizations for a pulsed CO EDL are presented and discussed. It is shown how all necessary parameters and quantities of interest can be scaled to analyze a specific problem in terms of more general classes of results. The sensitivity of the system response and the characterization of the gain saturation as a function of total radiation intensity are investigated. It is shown that the transient quantum energy and power conversion efficiencies are, to a good approximation, mainly dependent only upon the total energy deposition as a function of time. For typical cases of interest, the scaled cavity loss coefficient is small enough that oscillation is high above threshold, and it is found that turn-on occurs (typically) after ~ 0.6 - 1.0 J/liter/torr has been deposited, and that steady state is attained after ~ 1.9 - 2.6 J/liter/torr has been deposited. (These energies increase approximately as $\tilde{W}_e^{1/6}$, where $\tilde{W}_e = W_e / p_{CO}^2$). At steady state, the scaled total saturation intensity is ~ 0.6 - 6.4 W/cm²/torr² over the range of temperatures from 60-300°K.

1.0 INTRODUCTION

A molecular kinetic model for an electrically excited (CO , N_2 , Ar , He , ...) gas mixture has been constructed for the calculation of the radiative characteristics of a CO laser oscillator or amplifier. A computer program for the numerical solution of the steady state or transient master equation for the diatomic species has been developed to predict vibrational population distributions, gain and saturation parameters, energy transfer and extraction rates, conversion efficiencies, output intensities, and spectral distributions. The radiative calculations are self-consistent with the saturated gain on all oscillating transitions equal to the losses. The plasma characteristics, described by a Boltzmann distribution, are adjusted self-consistently in the calculations as a function of time to account for electron heating for a given temporal input power. A more complete discussion of the assumptions upon which this model are based has been given elsewhere^{1,2} and numerical results for a variety of operating conditions were presented and compared with experimental data from a pulsed high pressure E-beam stabilized electric discharge CO laser oscillator (EDL).¹ Furthermore, very good agreement has also been obtained in comparison of theoretical calculations from this model with results of transient gain relaxation measurements³ and with small-signal gain measurements over a large number of vibrational bands.

It is possible to make several reasonable approximations that allow certain general scaling laws for a CO EDL to be formulated. Because of the successful comparison of predictions of the theoretical model with experimental data from the E-beam pulsed device,¹ the results of scaling the transient analysis for an electrically excited pulsed CO oscillator will be presented here. These generalizations depend only upon a few basic scale parameters, which make it possible to predict the temporal output characteristics of a large class of systems. However, the present results are limited to gas mixtures containing CO and monotomic diluent gases

only. This restriction provides a considerable simplification insofar as the generalized results do not depend upon the ratio of two diatomic species present; moreover, it is necessary at the present time due to uncertainties in the (CO, N₂) and (N₂, N₂) cross-relaxation rates as a function of kinetic temperature and vibrational quantum numbers.

2.0 MOLECULAR KINETIC MODEL: SUMMARY

The physics of the present theoretical model that is used to predict the characteristics of a transient pulsed electrically excited CO laser oscillator is described by four basic systems of equations that couple the CO vibrational state population densities, the radiation intensities, the gas kinetic temperature, and the plasma kinetic parameters (electron density and temperature) as a function of time. The general formulation of these equations and assumptions made will be briefly summarized here, and it will be shown where certain approximations (most of which are not required for the complete computer analysis, however) make it possible to obtain essential results in terms of a very small set of scale parameters. In fact, two basic parameters related to pumping and cavity loss are all that will be required to present a very generalized description of the (CO, X) EDL under the set of approximations to be discussed below.

The physics of the molecular kinetic processes is described by the master equation for the vibrational population densities n_v of the CO molecule,

$$\begin{aligned} \frac{dn_v}{dt} = & n_e \sum_{v'} [n_{v'} \langle v(E) \sigma_{v' \rightarrow v}(E) \rangle - n_v \langle v(E) \sigma_{v \rightarrow v'}(E) \rangle] + \\ & \sum_X N_X [P_{v+1 \rightarrow v}^{VT}(\text{CO}, X) n_{v+1} - P_{v \rightarrow v+1}^{VT}(\text{CO}, X) n_v \\ & - P_{v \rightarrow v-1}^{VT}(\text{CO}, X) n_v + P_{v-1 \rightarrow v}^{VT}(\text{CO}, X) n_{v-1}] + \\ & \sum_{v'} [P_{v+1, v'-1 \rightarrow v, v'}^{VVT} n_{v+1} n_{v'-1} - n_v n_{v'} \times \\ & P_{v, v' \rightarrow v+1, v'-1}^{VVT} - P_{v, v' \rightarrow v-1, v'+1}^{VVT} n_v n_{v'}] + \end{aligned}$$

(continued)

$$\begin{aligned}
& P_{v-1, v'+1 \rightarrow v, v'}^{VVT} n_{v-1} n_{v'+1}] \\
& - n_v [A_{v \rightarrow v-1} + A_{v \rightarrow v-2}] + n_{v+2} A_{v+2 \rightarrow v} + n_{v+1} A_{v+1 \rightarrow v} \\
& - n_v S_{v \rightarrow v-1}^{stim} + n_{v-1} S_{v-1 \rightarrow v}^{stim} \\
& - n_v S_{v \rightarrow v+1}^{stim} + n_{v+1} S_{v+1 \rightarrow v}^{stim}
\end{aligned} \tag{1}$$

The pumping and relaxation processes include, in order of appearance: (1) electron impact excitation of the vibrational states, (2) vibration to translation (VT) deactivation processes, (3) near resonant vibration to vibration (VVT) single quantum exchange collisions, (4) spontaneous radiative decay, and (5) stimulated emission and absorption processes. P^{VVT} and P^{VT} represent $\langle v\sigma \rangle$ rates (in cm^3/s) for the VV and VT collision processes. In addition to the master equation for the vibrational population densities, assumptions must be introduced for calculation of the plasma parameters and radiation intensities as a function of time to theoretically characterize the CO EDL. The sources of the electrical excitation cross sections, VT and VVT cross-relaxation rates and theories, and radiative and molecular parameters used in the present model have been discussed elsewhere.^{1, 2}

The assumptions that are made for determination of the radiation intensities for an oscillator are the following. The rotational levels are assumed to be in thermal equilibrium with the molecular kinetic temperature, and rotational cross-relaxation is assumed to be

sufficiently fast that only one rotational line can oscillate in any given vibrational band. The gains for the $v \rightarrow v-1$ P(J) transition are given by

$$\alpha(v, J) = n_v \sigma_{21}(v, J) - n_{v-1} \sigma_{12}(v, J), \quad (2)$$

where $\sigma_{12}(v, J)$ and $\sigma_{21}(v, J)$ are the stimulated emission and absorption cross sections defined by

$$\sigma_{21}(v, J) = \frac{S(\nu_v^J) \tilde{\nu}_v^J A_{10} B_{vJ}}{8\pi kT \tilde{\nu}_{10}^3} |R_{v,v-1}/R_{10}|^2 \exp\{-B_v J(J-1)/kT\}$$

$$\sigma_{12}(v, J) = \frac{S(\nu_v^J) \tilde{\nu}_v^J A_{10} B_{v-1J}}{8\pi kT \tilde{\nu}_{10}^3} |R_{v,v-1}/R_{10}|^2 \exp\{-B_{v-1} J(J+1)/kT\} \quad (3)$$

Losses such as mirror absorption, output coupling, window losses, or intracavity line selection losses are all assumed to be uniformly distributed throughout the laser gain medium. These cavity losses are assumed to be small enough that the approximation of a spatially uniform intensity distribution over the length of the active medium is adequate for describing the molecular and radiative characteristics of the medium. The optical resonator is assumed to be formed by two plane parallel mirrors (one totally reflecting, the other with reflectivity R) separated by a distance L . From the threshold condition, $R \exp[2(\alpha - \beta)L] = 1$, the gain coefficient α for an oscillating line (for $R \approx 1$) is given by $\alpha = \beta + (1 - R)/2L$, where β is the loss

coefficient for the cavity exclusive of the output coupling. The percentage of the total radiative conversion of electrical energy that can be extracted as output (assuming $\beta = \text{constant}$ for all lines) is given by the coupling efficiency $(T/2)/(\beta L + T/2)$, where T is the mirror transmission. Radiation intensities are calculated by requiring that the gain coefficients $\alpha(v, J)$ of all oscillating transitions be equal to the loss coefficient γ at all times:

$$\sigma_{21}(v, J) n_v(t) - \sigma_{12}(v, J) n_{v-1}(t) = \beta + T/2L = \gamma \quad (4)$$

Thus, if at time t a set of transitions (v, J_v) have just attained (or continue to have) gain at threshold, their intensities $I_v(t)$ must satisfy a simultaneous set of equations of the form

$$\begin{aligned} \sigma_{21}(v, J_v) \dot{n}_v(t) - \sigma_{12}(v, J_v) \dot{n}_{v-1}(t) = \\ -T [n_v(t) d\sigma_{21}(v, J_v)/dT - n_{v-1}(t) d\sigma_{12}(v, J_v)/dT] \end{aligned} \quad (5)$$

The intensities $I_v(t)$ enter Eq. (5) upon substitution of the master Eq. (1) for $n_v(t)$,

$$\dot{n}_v(t) = R_v(t) + \gamma \left[\frac{I_{v+1}(t)}{h\nu(v+1, J_{v+1})} - \frac{I_v(t)}{h\nu(v, J_v)} \right] \quad (6)$$

which is here shown separated explicitly into the nonradiative kinetic terms $R_v(t)$ and stimulated emission and absorption terms. The stimulated emission and absorption rates $S_{v \rightarrow v-1}^{\text{stim}}$ and $S_{v-1 \rightarrow v}^{\text{stim}}$ that occur in Eq. (1) can be expressed in terms of the cross sections defined by Eq. (3) and the radiation intensities $I_v^J(t)$ by the relations

Combination of Eq. (8) - (10) gives a relation for determining the effective electron temperature $T_e(t)$ as a function of time.

If the master Eq. (1) is multiplied by the vibrational energy E_v and summed over the levels v , an equation for the conservation of power per unit volume is obtained:

$$\begin{aligned} dE_{vib}(t)/dt = & W_e(t) + W_{VV}(t) + W_{VT}(t) + W_{spon}(t) \\ & + [W_{stim}(t) + W_{rot}(t)] \end{aligned} \quad (11)$$

where $E_{vib}(t)$ is the total stored vibrational energy density, $W_e(t)$ is the electrical power into vibrational excitation defined by Eq. (10), $W_{VV}(t)$ and $W_{VT}(t)$ are the net powers converted to kinetic heating by VV and VT collision processes, $W_{spon}(t)$ is fluorescence power, W_{stim} is power converted to stimulated radiation (either extracted or absorbed), and $W_{rot}(t)$ is power converted to kinetic heating by rotational cross-relaxation. The last two terms are shown grouped together, since the origin of the rotational heating $W_{rot}(t)$ is the change of J level that occurs with lasing: since stimulated emission and absorption of radiation occur on P(J) transitions, the assumptions of fast rotational cross relaxation and rotational thermal equilibrium with the kinetic temperature imply that the rotational energy change that results from $(J-1 \rightarrow J)$ is instantaneously converted to heat.

Explicit expressions for the terms occurring in Eq. (11) are given by

$$W_{stim}(t) = \gamma \sum_v I_v(t) = \gamma I(t) \quad (12)$$

$$\begin{aligned}
W_{VV}(t) &= \sum_{v, v'} (E_v - E_{v'}) [n_v n_{v'-1} P_{v, v'-1 \rightarrow v-1, v'}^{VVT} \\
&\quad - n_{v-1} n_{v'} P_{v-1, v' \rightarrow v, v'-1}^{VVT}] \quad (13)
\end{aligned}$$

$$\begin{aligned}
W_{VT}(t) &= \sum_{X, v} (E_v - E_{v-1}) [n_v P_{v \rightarrow v-1}^{VT}(\text{CO}, X) \\
&\quad - n_{v-1} P_{v-1 \rightarrow v}^{VT}(\text{CO}, X)] N_X \quad (14)
\end{aligned}$$

$$\begin{aligned}
W_{\text{rot}}(t) &= \sum_v (E_v - E_{v-1}) [n_v S_{v \rightarrow v-1}^{\text{stim}} - n_{v-1} S_{v-1 \rightarrow v}^{\text{stim}}] \\
&\quad - W_{\text{stim}}(t) \quad (15)
\end{aligned}$$

The gas kinetic temperature increases as a function of time, due to the conversion of input power to kinetic heating:

$$\begin{aligned}
[N_{\text{CO}} + (3/2) N_{\text{tot}}] kT &= W_{VV}(t) + W_{VT}(t) \\
&\quad + W_{\text{rot}}(t) \equiv W_H(t) \quad (16)
\end{aligned}$$

3.0 APPROXIMATIONS AND SCALING GENERALIZATIONS

In order to derive a useful set of generalized results that can be easily scaled, it is first necessary to simplify the sets of equations presented in the previous section by introducing approximations that will reduce the number of scale parameters required to a reasonable minimum value. Although the additional approximations to be discussed here are neither required nor invoked in the complete computer analysis, they will be useful for summarizing the results of computer calculations in a coherent way. Clearly, it will always be possible to characterize any particular class of problems by a suitably large set of parameters, so the objective here will be to show that a rather general class of pulsed CO oscillators (containing CO and monatomic gases only) can be described quite accurately in terms of only two basic scale parameters that define the electrical pumping and cavity threshold.

For a high pressure oscillator (i.e., > 20 torr) operating at temperatures typically in the range ~ 60 - 300°K , the spontaneous radiation and VT decay terms in the master equation (1) can, to a very good approximation, be neglected. Consistent with this approximation, the contribution $W_{VT}(t)$ to the kinetic heating that occurs in the temperature Eq. (16) can also be neglected. It will be convenient to refer to the initial values of the temperature (T_{mol}) and pressures (p_{CO} , p_X ...) in the results of calculations to be presented here. Only a small percentage of electrical power is converted to kinetic heating (typically $< 10\%$ even after steady state has been attained, so (for reasonably dilute CO gas mixtures) it is a good approximation to neglect the temperature rise for pulse times that are comparable to the time required to reach steady state. Thus, although the calculations correspond to the situation for which the gas number densities are fixed, the pressures

(for such cases) will change by only a small fraction during that time scale. In any case, nothing is sacrificed by the choice of the initial values of these quantities to form the scale parameters, and the heating considerations will be made more precise below. All of the calculations to be presented here correspond to cases for which the electrical excitation was kept constant as a function of time during the pulse -- i.e., $t_r = 0$, and $t_f = \infty$, with adjustment of the electron temperature T_e .

We shall now show how the coupled set of equations discussed in the previous section can be rewritten in a more useful form by introducing the following quantities:

$$\begin{aligned}
 x_v &= n_v / N_{CO} \\
 x_e &= n_e / N_{CO} \\
 \tau &= p_{CO} t \\
 f &= 1 + (3/2) p_{tot} / p_{CO} \\
 \xi &= \frac{p_{CO} \langle v_{rel}(CO, CO) \rangle \sigma^{opt}(CO, CO)}{\sum_X p_X \langle v_{rel}(CO, X) \rangle \sigma^{opt}(CO, X)} \\
 \tilde{P}_{v, v' \rightarrow v-1, v'+1}^{VVT} &= P_{v, v' \rightarrow v-1, v'+1}^{VVT} / (kT_{mol}) \\
 \tilde{\sigma}_{v \rightarrow v'} &= \sigma_{v \rightarrow v'} / (kT_{mol}) \\
 \tilde{\sigma}(v, J) &= \sigma(v, J) p_{CO} / \xi \\
 \tilde{\gamma} &= \gamma / \xi \\
 \tilde{W} &= W / p_{CO}^2 \\
 \tilde{I} &= I \xi / p_{CO}^2 \\
 \tilde{E}_{vib} &= E_{vib} / p_{CO}
 \end{aligned} \tag{17}$$

The physical significance of these parameters is readily apparent: x_v are the relative populations, x_e is a measure of the degree of ionization, f is related to the number of thermal degrees of freedom, ξ is the fractional percentage of optical line broadening caused by CO, \tilde{P}^{VVT} and $\langle v \tilde{\sigma}_{v \rightarrow v'} \rangle$ are (proportional to) the VV and electrical excitation rates in units of $s^{-1} \text{ torr}^{-1}$, $\tilde{\sigma}(v, J)$ is proportional to the stimulated emission cross section with dependence on pressures removed, and $\tilde{\gamma}$, \tilde{W} , \tilde{I} and \tilde{E} are scaled threshold loss, power, intensity and energy. It is assumed that pressures are high enough (≥ 20 torr) that optical lines are predominantly pressure broadened, so that the definition of the parameter ξ is meaningful.

Since the VT collision and spontaneous radiation terms are now to be neglected, the master Eq. (1) becomes

$$\begin{aligned} x'_v(\tau) = & x_e \sum_{v'} [x_{v'} \langle v \tilde{\sigma}_{v' \rightarrow v} \rangle - x_v \langle v \tilde{\sigma}_{v \rightarrow v'} \rangle] \\ & + \sum_{v, v'} [\tilde{P}_{v+1, v'-1 \rightarrow v, v'}^{VVT} x_{v+1} x_{v-1} + \dots] \\ & - x_v \tilde{\sigma}_{21}(v, J) \tilde{I}_v / h\nu_v^J + x_{v-1} \tilde{\sigma}_{12}(v, J) \tilde{I}_v / h\nu_v^J + \dots \quad (18) \end{aligned}$$

where the prime (') denotes differentiation with respect to τ , and where the electrical excitation term can be written in terms of the scaled electrical pumping power \tilde{W}_e by eliminating the relative ionization parameter x_e :

$$x_e = \tilde{W}_e \left[\sum_{v, v'} E_v (x_v \langle v \tilde{\sigma}_{v \rightarrow v'} \rangle - x_{v'} \langle v \tilde{\sigma}_{v' \rightarrow v} \rangle) \right]^{-1} \quad (19)$$

Thus, the master equation expresses the evolution of the relative populations x_v as a function of scale time $\tau = p_{CO} t$. This is to be

expected, since the electrical excitation is kept constant, and the dominant kinetic processes are (two body) VV collisions. Eq. (18) shows that the physics of the molecular vibration states depends explicitly only upon the kinetic temperature and the scaled electrical excitation $\tilde{W}_e = W_e / p_{CO}^2$. Implicitly, however, it depends also the scaled threshold loss coefficient $\tilde{\gamma}$ for the cavity due to the oscillation condition (4), and upon the parameter f due to the kinetic heating Eq. (16). In terms of the parameters of (17), Eq. (4) and (16) become, respectively

$$[\tilde{\sigma}_{21}(v, J) x_v - \tilde{\sigma}_{12}(v, J) x_{v-1}] / (kT_{mol}) = \tilde{\gamma} \quad (20)$$

$$T' = \tilde{W}_H(\tau) T_{mol} / f \quad (21)$$

Eq. (15), which defines the intensities of the oscillating transitions, becomes

$$\begin{aligned} \tilde{\sigma}_{21}(v, J) x_v' - \tilde{\sigma}_{12}(v, J) x_{v-1}' = \\ -(\tilde{W}_H T_{mol} / f) [x_v d \tilde{\sigma}_{21}(v, J) / dT - x_{v-1} d \tilde{\sigma}_{12}(v, J) / dT] \end{aligned} \quad (22)$$

The power balance Eq. (11) becomes

$$d\tilde{E}_{vib}(\tau) / d\tau = \tilde{W}_e + \tilde{W}_{VV}(\tau) + \tilde{W}_{stim}(\tau) + \tilde{W}_{rot}(\tau) \quad (23)$$

It is apparent from Eq. (18) - (22) that the set of parameters $(T_{mol}, \tilde{W}_e, \tilde{\gamma}, f)$ completely characterizes the problem; all of the other (extensive) input consists of fundamental physical constants. In the following section, a variety of numerical results based on the complete computer analysis for this model will be presented and discussed to show the relative sensitivity of these parameters.

4.0 DISCUSSION AND NUMERICAL RESULTS

The computer calculations that have been carried out correspond to a fixed value $f = 16$ (corresponding to a dilute, 10% CO mixture). The kinetic temperatures T_{mol} include (60, 100, 150, 200, 300) °K, the scaled electrical pumping rates (0.2, 0.5, 1.0, 2.0, 5.0, 10, 20, 50, 100, 200) $\text{W}/\text{cm}^3/\text{torr}^2$, and the scaled threshold loss coefficients (0.1, 0.2, 0.5, 1.0, 3.0, 7.0, 10, 20) %/cm. From the results of any given case specified completely by the set of four parameters (T_{mol} , \tilde{W}_e , $\tilde{\gamma}$, f), the general class of problems that can be scaled directly from those results is quite restrictive; it allows only the variation of the CO partial pressure, provided that the electrical excitation W_e is scaled by p_{CO}^2 , and that the threshold level and gas mixture ratio are held constant. However, except for the scaled excitation power \tilde{W}_e , most of these parameters do not have a sensitive effect on the power response of the system as a function of time (although detailed spectral predictions may have a more critical dependence). Thus, the class of problems that can be analyzed from a given case is often more extensive than that just described. The reasons for this are the following: (1) the most important parameter, the scaled excitation \tilde{W}_e , is a measure of the electrical pumping per molecule relative to the rate of VV cross-relaxation, and thus specifies the ratio of the two dominant kinetic processes in the CO EDL. (2) A pulsed high pressure CO EDL typically operates in a regime where oscillation is high above threshold, and thus, results for optical power extraction will usually be insensitive to the scaled cavity loss coefficient $\tilde{\gamma}$. Unless the ratio $\tilde{W}_e / \tilde{\gamma}$ becomes very small (to be discussed more quantitatively below), the medium intensity will be high above the saturation intensity, and the optical output will be independent of $\tilde{\gamma}$. (3) Only small percentages of electrical input power are converted to kinetic heating (typically < 10%) even after steady state

has been attained, so it is a good approximation (for reasonably dilute CO mixtures) to neglect the temperature rise for pulse times comparable to the time required to reach steady state. That is, the results do not depend critically upon f , providing it is large (in which case, the right hand side of Eq. (21) and (22) can be neglected). (4) Results of calculations for systems operating with parameters in the above ranges do not show a significant sensitivity to dependence on T_{mol} .

Figure 1-8 show plots of the quantum power efficiency (for the total optical conversion of electrical input) for a variety of different values of T_{mol} , $\tilde{\gamma}$, and \tilde{W}_e as a function of $p_{\text{CO}} t$. As these families of curves show, the most important parameter for small values of $\tilde{\gamma}$ is the scaled excitation power \tilde{W}_e . Figure 9 displays a family of curves for which T_{mol} and \tilde{W}_e are fixed, with the efficiency η plotted as a function of $p_{\text{CO}} t$ for several values of $\tilde{\gamma}$; these show that the optical output is relatively insensitive for small values of this parameter. In fact, Figure 9 suggests at least semi-quantitatively that the response at 100°K is approximately independent of $\tilde{\gamma}$ if $\tilde{W}_e / \tilde{\gamma} \gtrsim 10 \text{ W/cm}^2 \text{ torr}^2$. This criterion will later be shown to be related to the scaled saturation intensity of the oscillator.

It is apparent from the set of Figures 1-9 that the optical output efficiency displays a remarkably similar behavior over a wide range of the parameters (\tilde{W}_e , T_{mol} , $\tilde{\gamma}$). In fact, these figures can be used to show that, for a given temperature T_0 and a fixed value of quantum efficiency η/η_∞ (where η_∞ is the steady state value), a loglog plot of $p_{\text{CO}} t$ versus the scaled power \tilde{W}_e is approximately linear. For example, Figures 10-13 show such plots for the turn-on time (obtained by extrapolating the curves of Figures 1-8 to the original and neglecting a small initial bump that often occurs in the calculations) versus \tilde{W}_e . The slope of these curves is approximately -5/6, and is independent of T_{mol} and $\tilde{\gamma}$; the variation in the magnitude of the curves is less than a factor of two within the

range of temperatures chosen. The turn-on time corresponds to the point where $\eta = 0$; however, it is apparent that the curves remain similar as time evolves. Thus, for a fixed temperature T_{mol} , the time t required to attain any specified value η/η_{∞} for the optical extraction efficiency satisfies

$$\tilde{e} = p_{\text{CO}} \tilde{W}_e^{5/6} = \text{const}, \quad (24)$$

which implies that, within a range of values for $\tilde{\gamma}$ which are suitably small, a "universal" plot of efficiency versus the parameter $\tilde{e} = p_{\text{CO}} \tilde{W}_e^{5/6}$ can be constructed. Several examples of such plots for different temperatures are shown in Figures 14-17. (Note that, as Figures 1-9 show, the value of the steady state efficiency η_{∞} depends only slightly upon \tilde{W}_e , T_{mol} , and $\tilde{\gamma}$.) The significance of the parameter \tilde{e} is obvious: if the exponent of \tilde{W}_e in Eq. (24) were unity instead of 5/6, \tilde{e} would represent the total electrical energy $\tilde{E} = W_e t / p_{\text{CO}}$ (J/cm³/torr) which has been deposited up to time t . Therefore, the response of the system is approximately a function only of the specific input energy \tilde{E} (which is, of course, a function of time and excitation rate). The power efficiency η/η_{∞} can be integrated to give a universal curve for the energy efficiency ϵ/η_{∞} as a function of the parameter \tilde{e} , and these results are presented in Figures 18-21.

Among the important conclusions to be drawn from the above remarks are the following. Characteristic times, such as turn-on time or time required to reach steady state, satisfy a relation given by Eq. (24). Figures 10-17 show that, for the range of temperatures and for the reasonably small values of $\tilde{\gamma}$ discussed here, turn-on occurs after a specific electrical energy $\tilde{E}_0 \sim 0.6 - 1.0$ J/liter/torr has been deposited, and steady state is attained after an energy $\tilde{E}_{\text{ss}} \sim 1.9 - 2.6$ J/liter/torr has been deposited. These numbers correspond to a specific pumping

rate $\tilde{W}_e = 1.0 \text{ W/cm}^3/\text{torr}^2$; for other values of \tilde{W}_e , Eq. (24) shows that these deposition energies increase as $\tilde{W}_e^{1/6}$. (Note that $1.0 \text{ J/liter/torr} = 7.6$ is a dimensionless number).

The kinetic temperature rise for pulse times comparable to the steady state time can be kept very small, provided that the gas mixture is reasonably dilute (corresponding to a large value for f). However, the parameter f does not affect the results critically, and is mainly important for detailed predictions of spectral distribution. To give some measure of the sensitivity of this parameter, Eq. (21) can be integrated to the steady state time. For all of the cases studied, the total energy converted to kinetic heating is very small, typically $\leq 5\%$ of the electrical input. Thus, at steady state, the temperature rise ΔT_{ss} will be

$$f \Delta T_{ss} / T_{mol} \leq .05 \tilde{E}_{ss} \approx 0.8 \quad (25)$$

Since the present calculations were carried out for $f = 16$, this condition predicts a total temperature rise limited to $\leq 5\%$. Clearly, the gross characteristics of the power output are not sensitive to such small temperature variations, so f can be varied by perhaps as much as a factor of 4 (at least for lower temperatures T_{mol}). No detailed investigation has been made of the effects on output spectral distribution.

It is interesting to characterize the CO medium by a saturation intensity. Although the full kinetic model contains oscillation on several lines simultaneously, it is convenient to neglect this feature for the moment, and observe how the gain saturates as a function of the total intensity

in the medium. From the analysis of a simple two-level model, it can be shown² that the saturated gain $\alpha(I)$ satisfies

$$\alpha(I) = \alpha_0 (1 + I/I_s)^{-1}, \quad (26)$$

where the saturation intensity I_s is independent of the electrical pumping. We shall show that, at steady state, the CO EDL follows a simple dependence of this form, and an estimate of the scaled saturation intensity as a function of T_{mol} will be derived. In terms of scaled quantities, Eq. (26) becomes, upon setting $\alpha(I) = \gamma$,

$$\tilde{\gamma} + \tilde{\gamma} \tilde{I}/\tilde{I}_s = \tilde{\alpha}_0. \quad (27)$$

At steady state, $\tilde{\gamma} \tilde{I} = \eta_\infty \tilde{W}_e$, and thus,

$$\tilde{\gamma} + \eta_\infty \tilde{W}_e / \tilde{I}_s = \tilde{\alpha}_0 \quad (29)$$

This equation shows that, for a fixed value of \tilde{W}_e , the steady state power efficiency η_∞ and the cavity threshold $\tilde{\gamma}$ are linearly related. That is, if $\eta_\infty(0)$ is the limiting value of the efficiency as $\tilde{\gamma} \rightarrow 0$, then

$$\tilde{\gamma} = - \left(\eta_\infty - \eta_\infty(0) \right) \tilde{W}_e / \tilde{I}_s \quad (29)$$

Figure 22 shows η_∞ plotted versus $\tilde{\gamma}$ for $T_{\text{mol}} = 100^\circ\text{K}$, for two different values of \tilde{W}_e , and as Eq. (29) shows, the slope $|d\tilde{\gamma}/d\eta_\infty|$ of these curves is proportional to \tilde{W}_e . Furthermore, the proportionality constant determines the scaled saturation intensity, which is determined from Figure 22 to be $\tilde{I}_s \sim 0.8 \text{ W/cm}^2/\text{torr}^2$. Similar plots for a fixed value of \tilde{W}_e and variable temperature T_{mol} are shown in Figure 23. All of these curves are linear to a very good approximation, and the saturation intensities obtained from their slopes are summarized in Table I.

During the transient evolution, the relation between the quantum efficiency and the cavity threshold does not seem to follow a linear relationship, as the results of Figure 9 indicate. This case is shown in Figure 24, in which the efficiency curves for three values of $\tilde{\gamma}$ have been replotted, with efficiencies at specific values of $p_{CO}t$ plotted versus $\tilde{\gamma}$ alongside for comparison.

Table I. Scaled Saturation Intensity

$T_{mol} (^{\circ}K)$	60	100	150	200	300
$\tilde{I}_s (W/cm^2/torr^2)$	0.6	0.8	1.6	2.5	6.4

Small signal gain characteristics can be obtained from Eq. (28) with $\tilde{\gamma} = 0$. For values of pumping and cavity threshold considered here, it is apparent that the small signal gain is proportional to \tilde{W}_e ,

$$\tilde{\alpha}_o = \eta_{\infty}(0) \tilde{W}_e / \tilde{I}_s$$

For efficient operation of the oscillator (high above threshold), the necessary condition is $\tilde{\alpha}_o \gg \tilde{\gamma}$, and therefore (since $\eta_{\infty} \sim 1$),

$$\tilde{W}_e / \tilde{\gamma} \gg \tilde{I}_s.$$

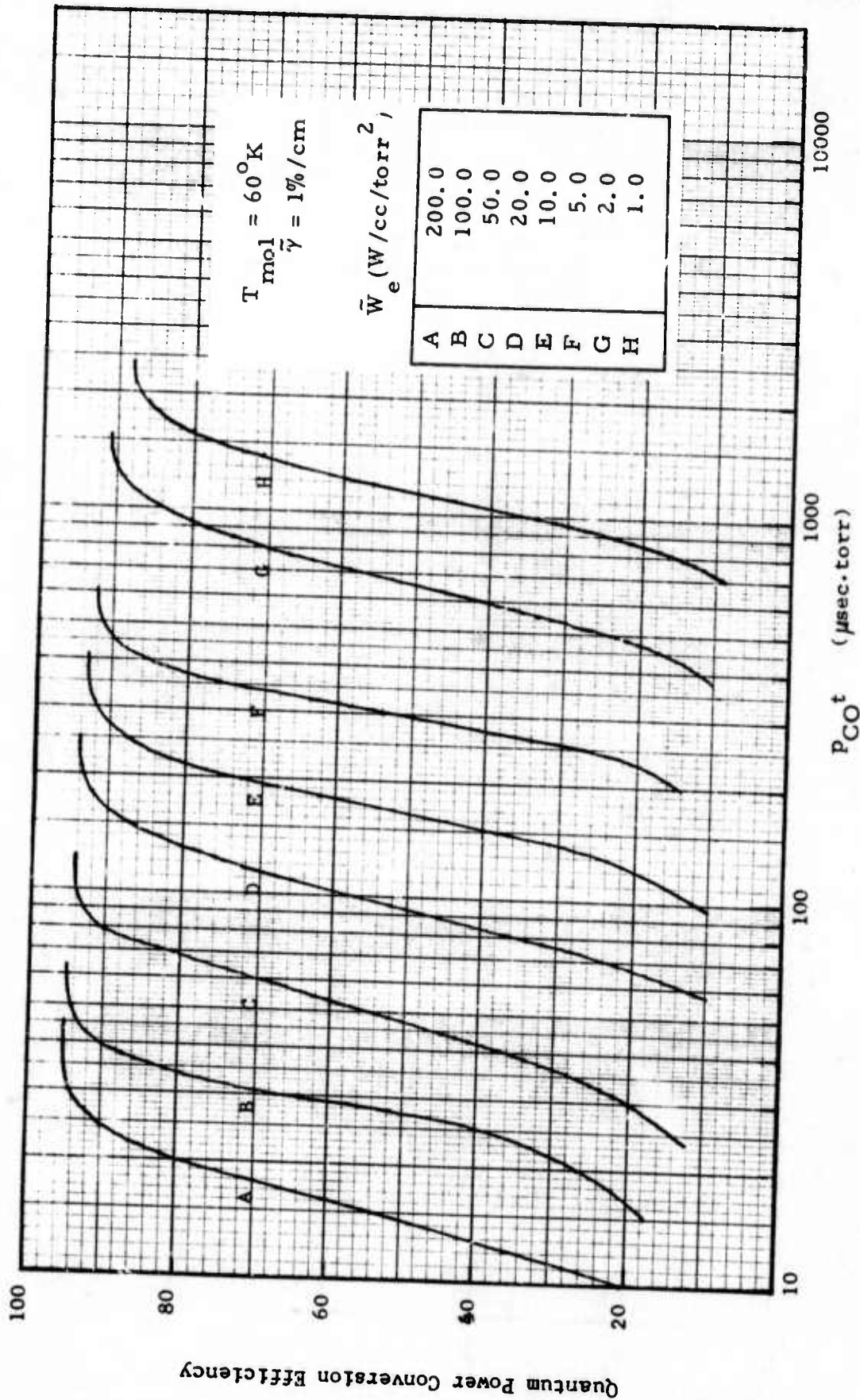


Figure 1. Quantum efficiency as a function of scale time P_{CO}^t for several values of scaled electrical pumping power.

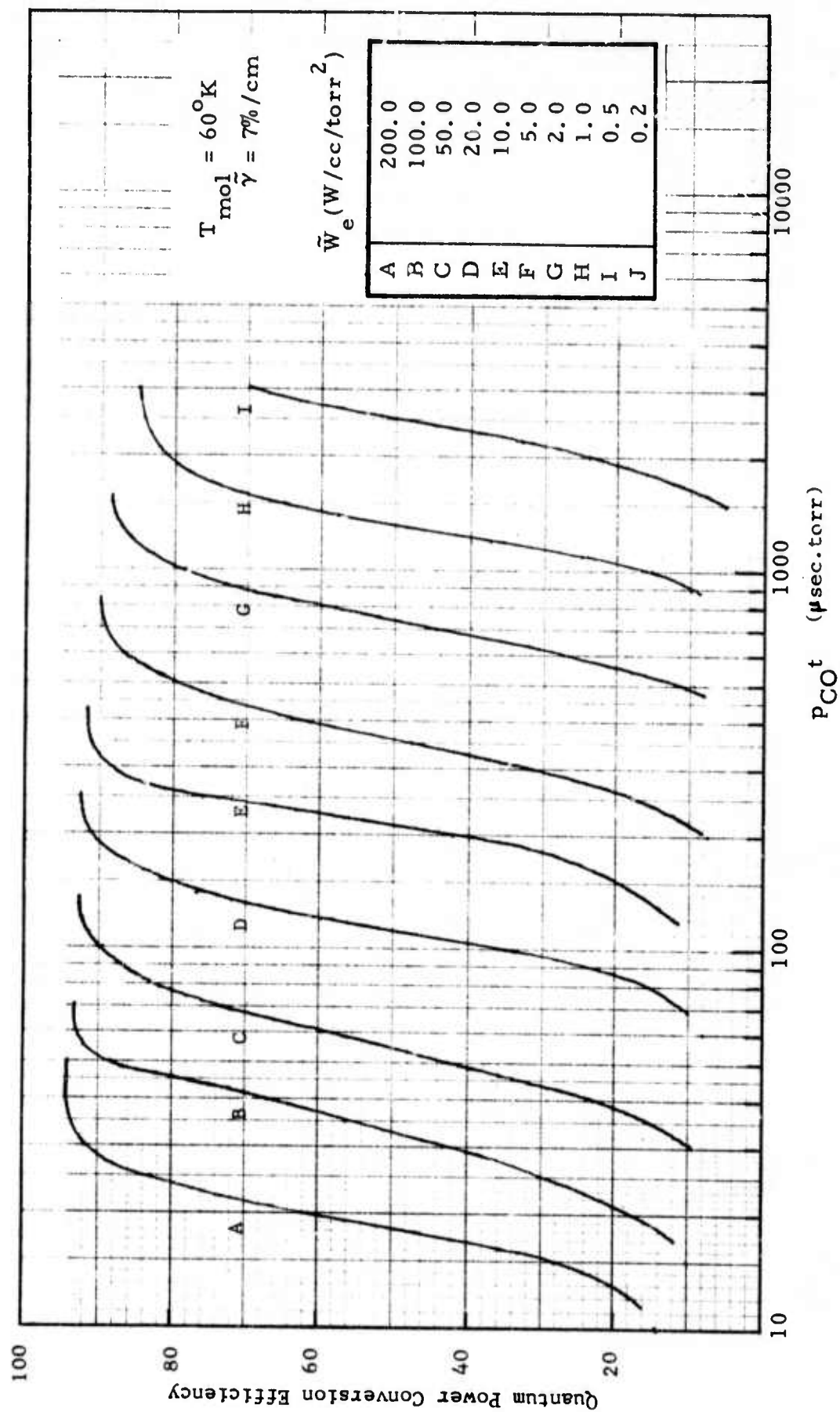


Figure 2. Quantum efficiency as a function of scale time p_{CO}^t for several values of scaled electrical pumping power.

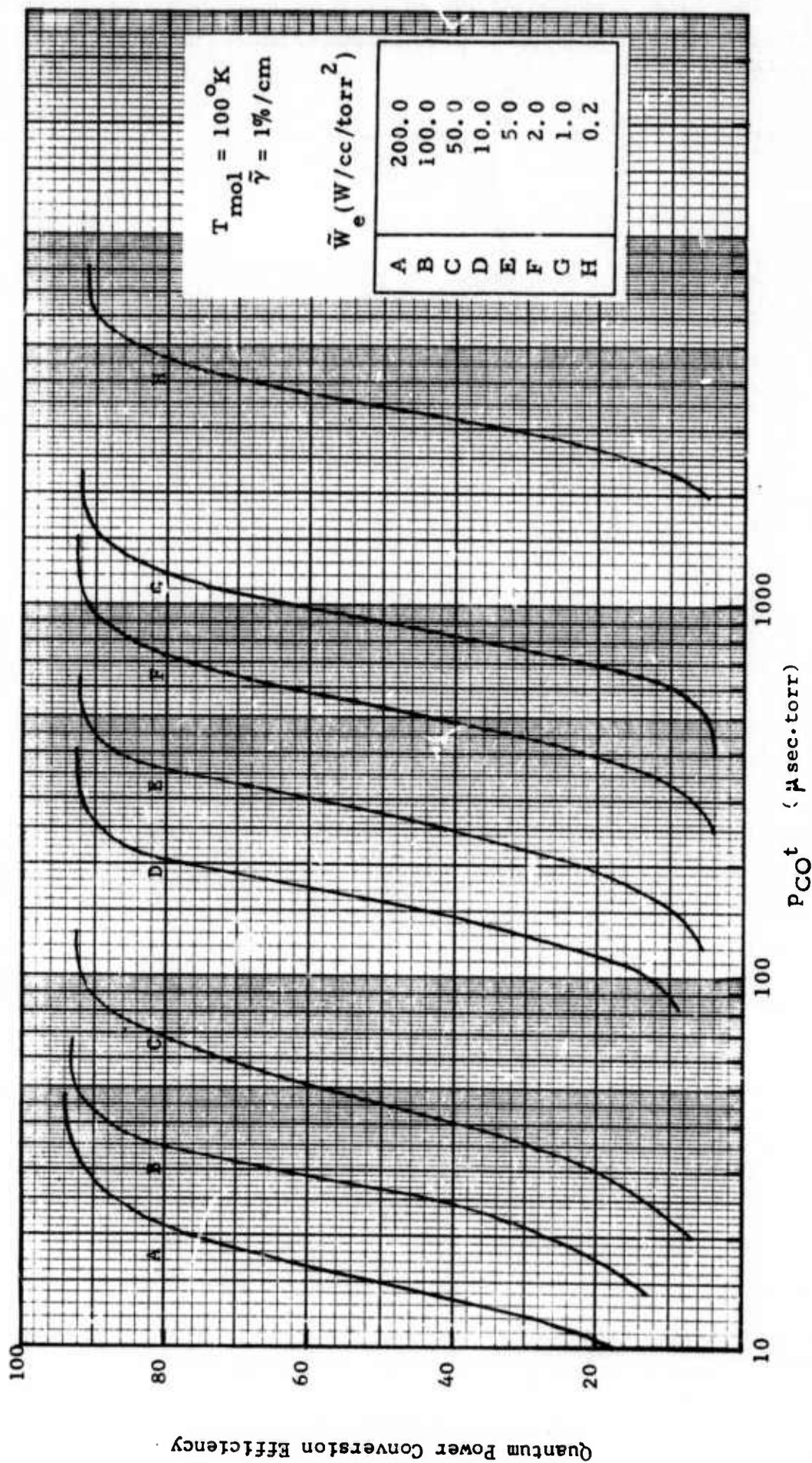


Figure 3. Quantum efficiency as a function of scale time P_{CO}^t for several values of scaled electrical pumping power.

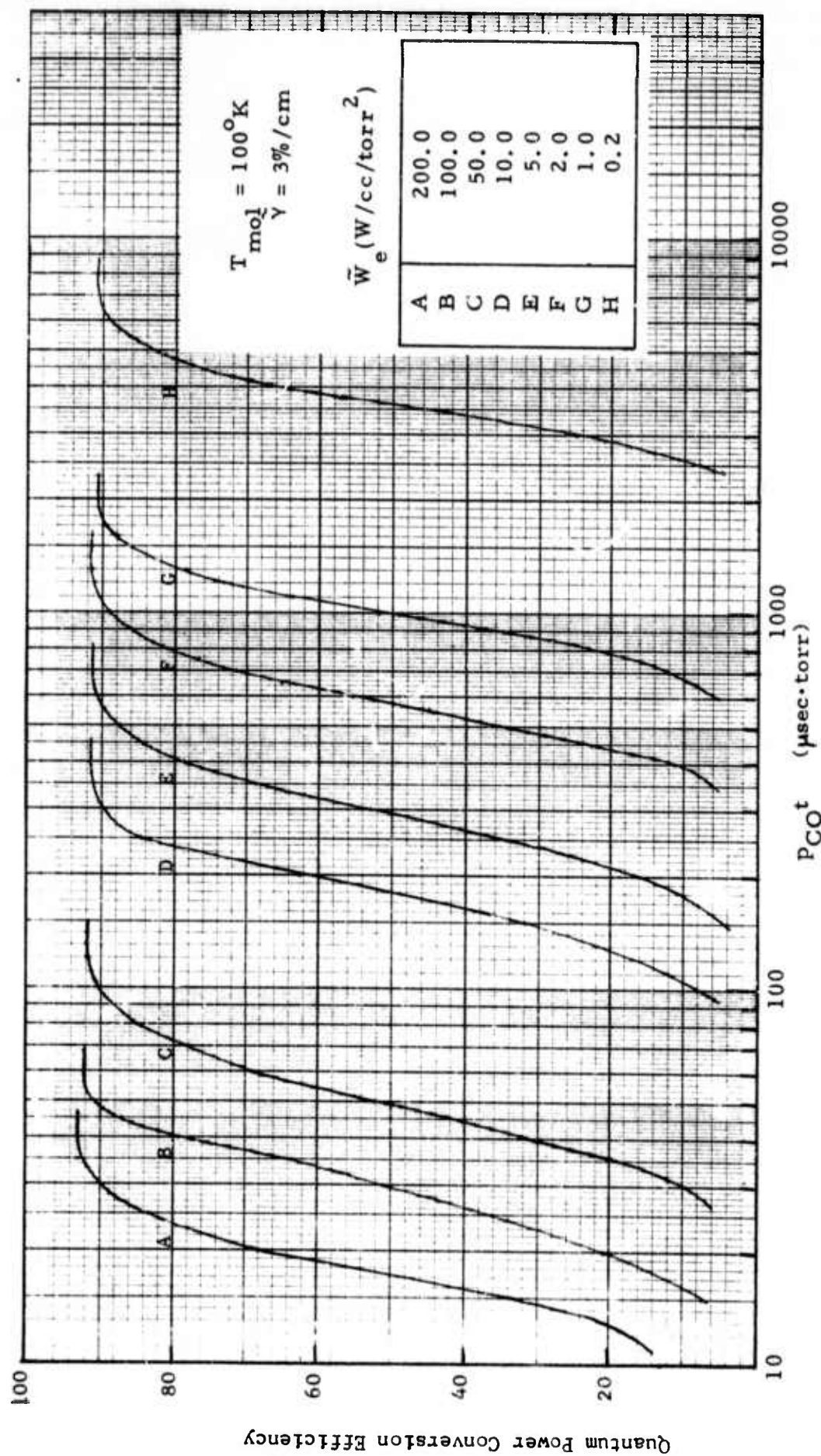


Figure 4. Quantum efficiency as a function of scale time $p_{\text{CO}} t$ for several values of scaled electrical pumping power.

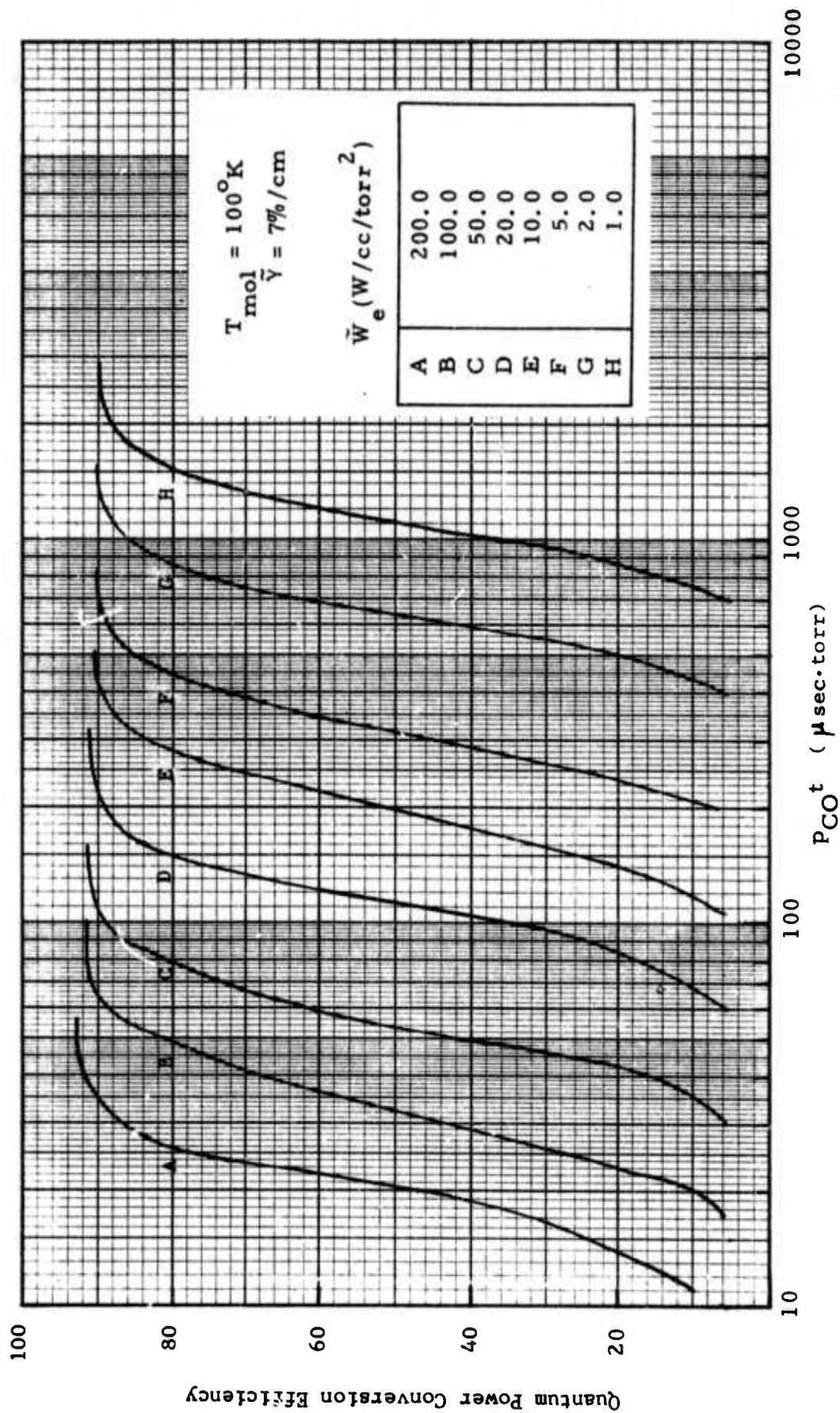


Figure 5. Quantum efficiency as a function of scale time $p_{\text{CO}} t$ for several values of scaled electrical pumping power.

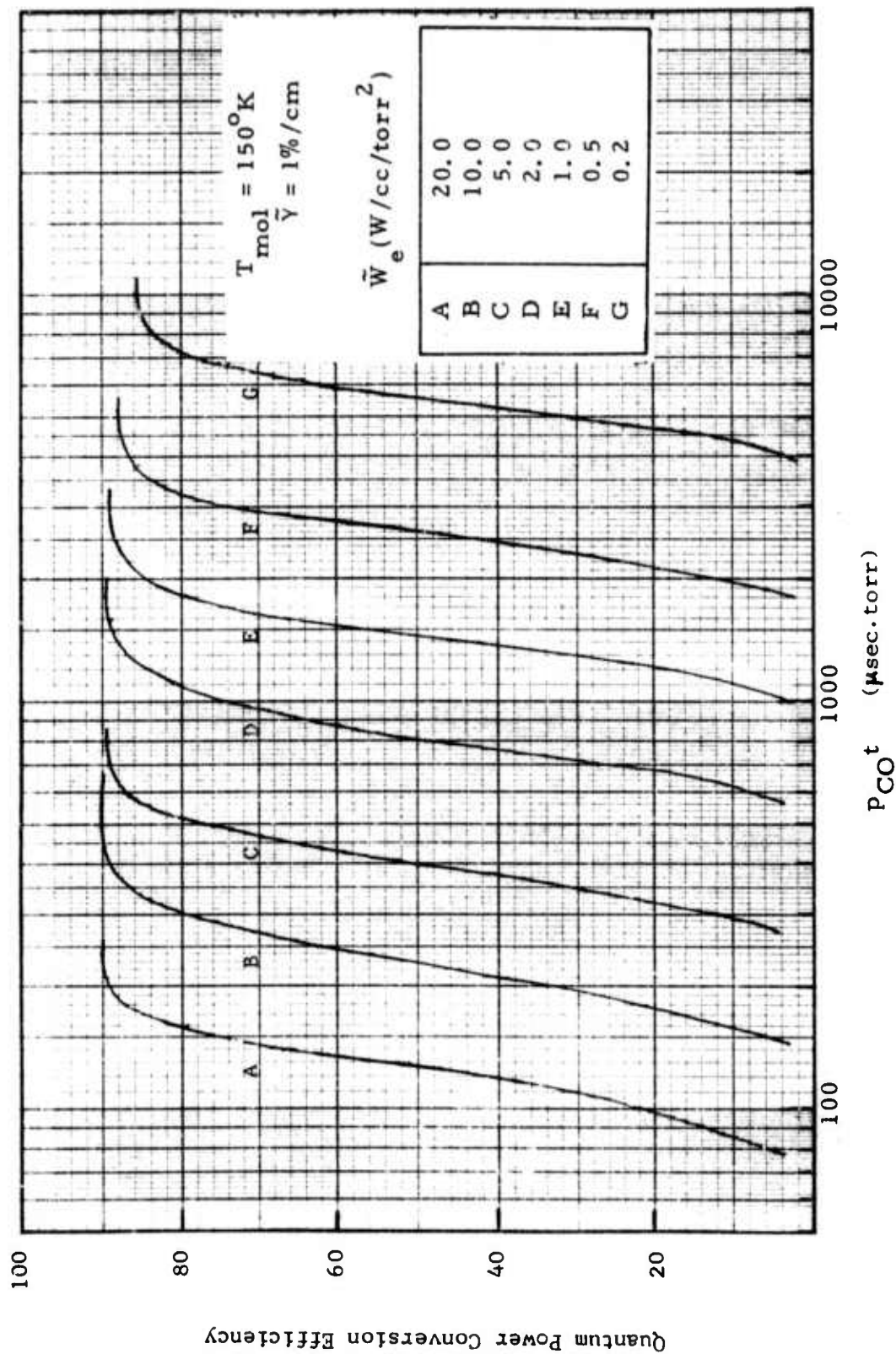


Figure 6. Quantum efficiency as a function of scale time $P_{\text{CO}} t$ for several values of scaled electrical pumping power.

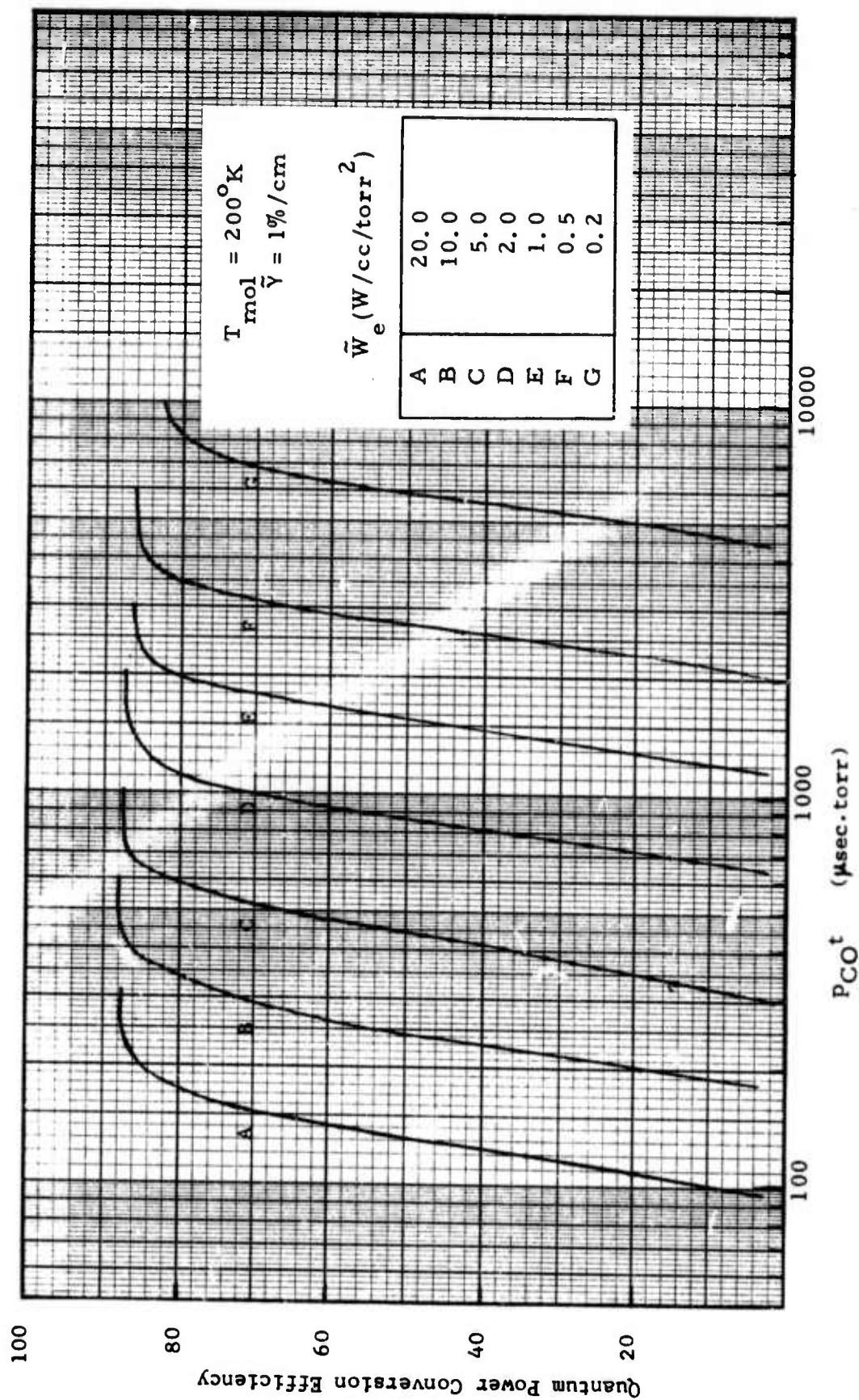


Figure 7. Quantum efficiency as a function of scale time P_{CO}^t for several values of scaled electrical pumping power.

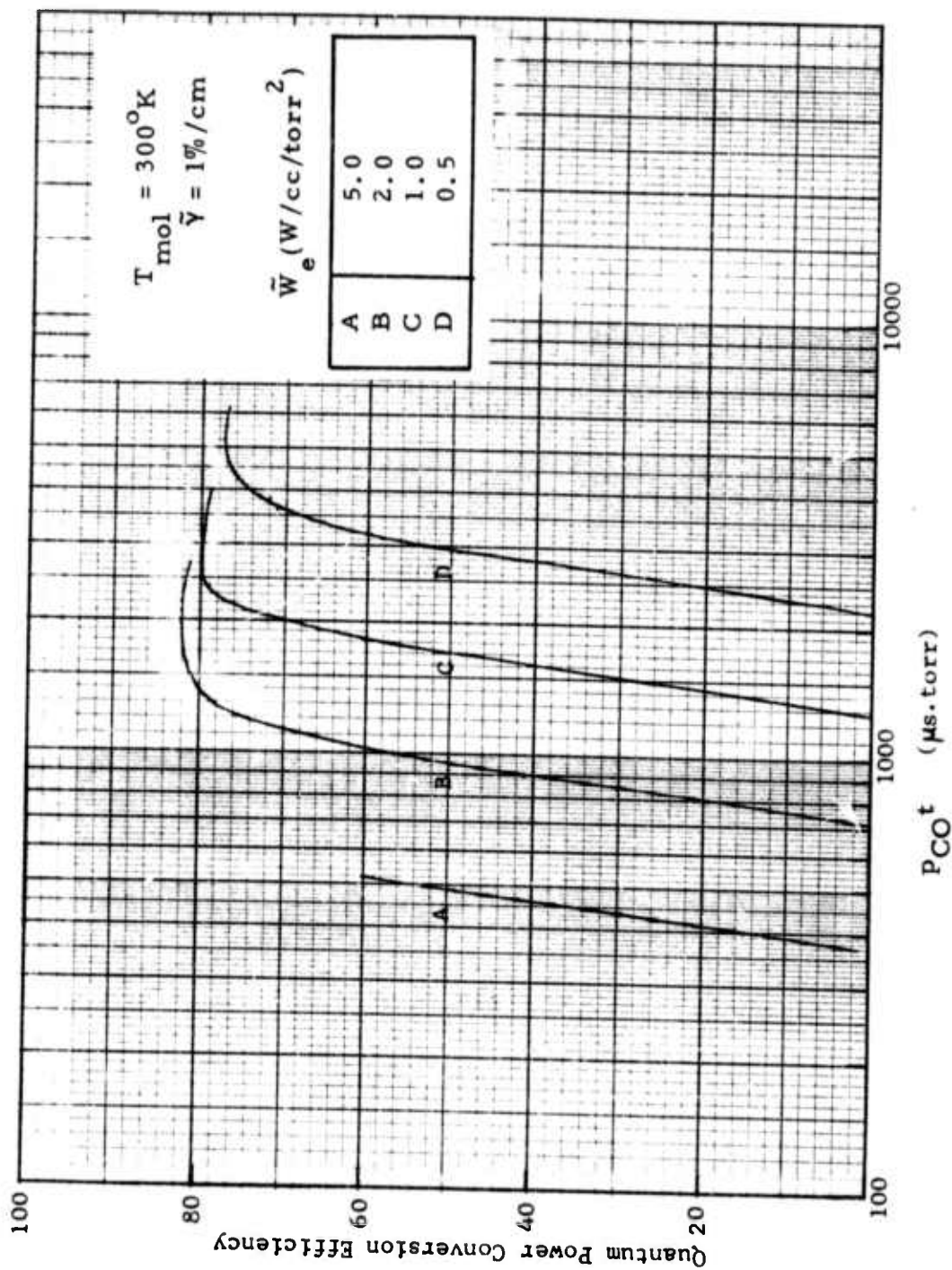


Figure 8. Quantum Efficiency as a function of scale time $P_{\text{CO}} t$ for several values of scaled electrical pumping power.

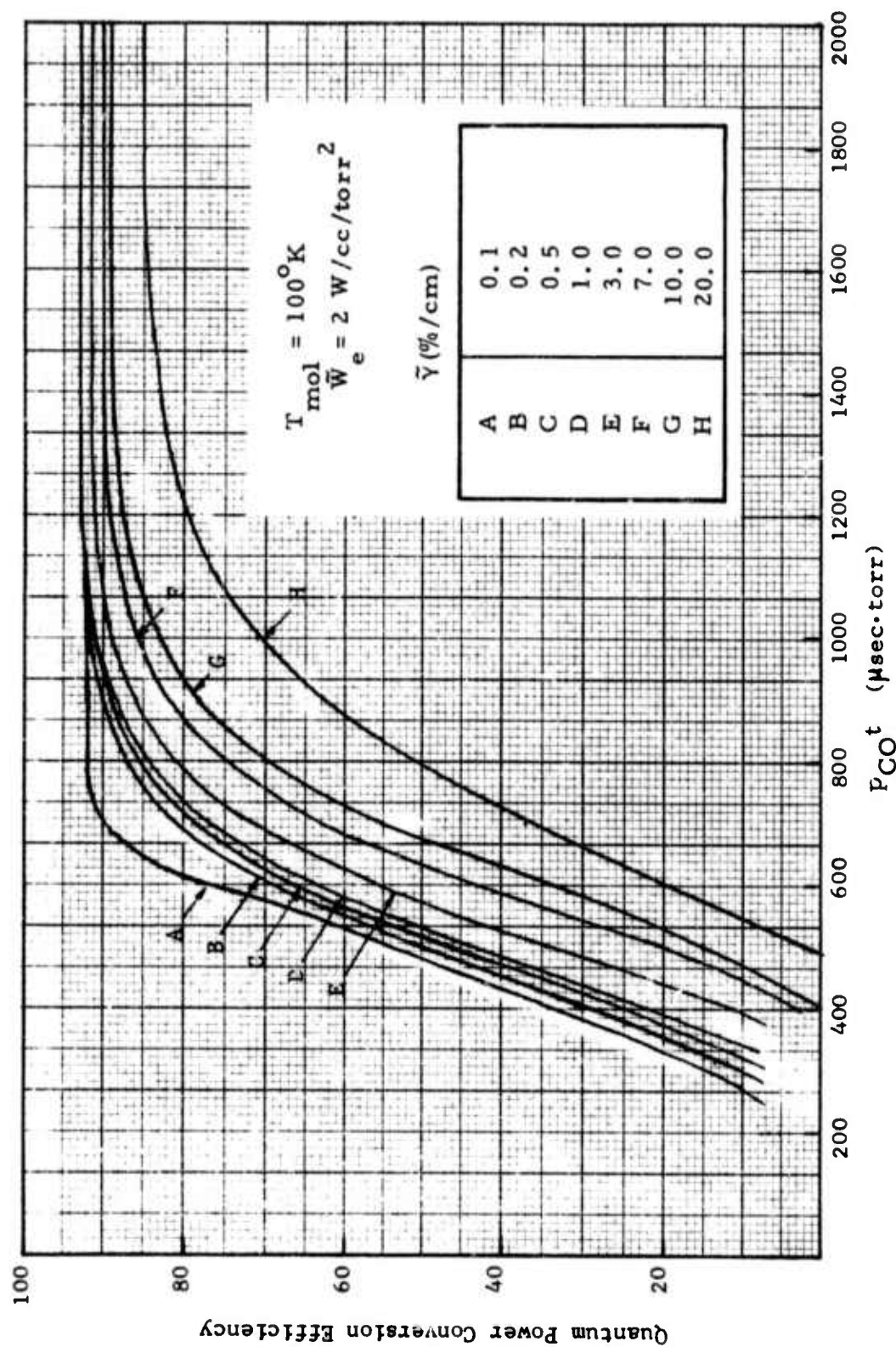


Figure 9. Quantum efficiency as a function of scale time P_{CO}^t for several values of scaled threshold loss $\tilde{\gamma}$.

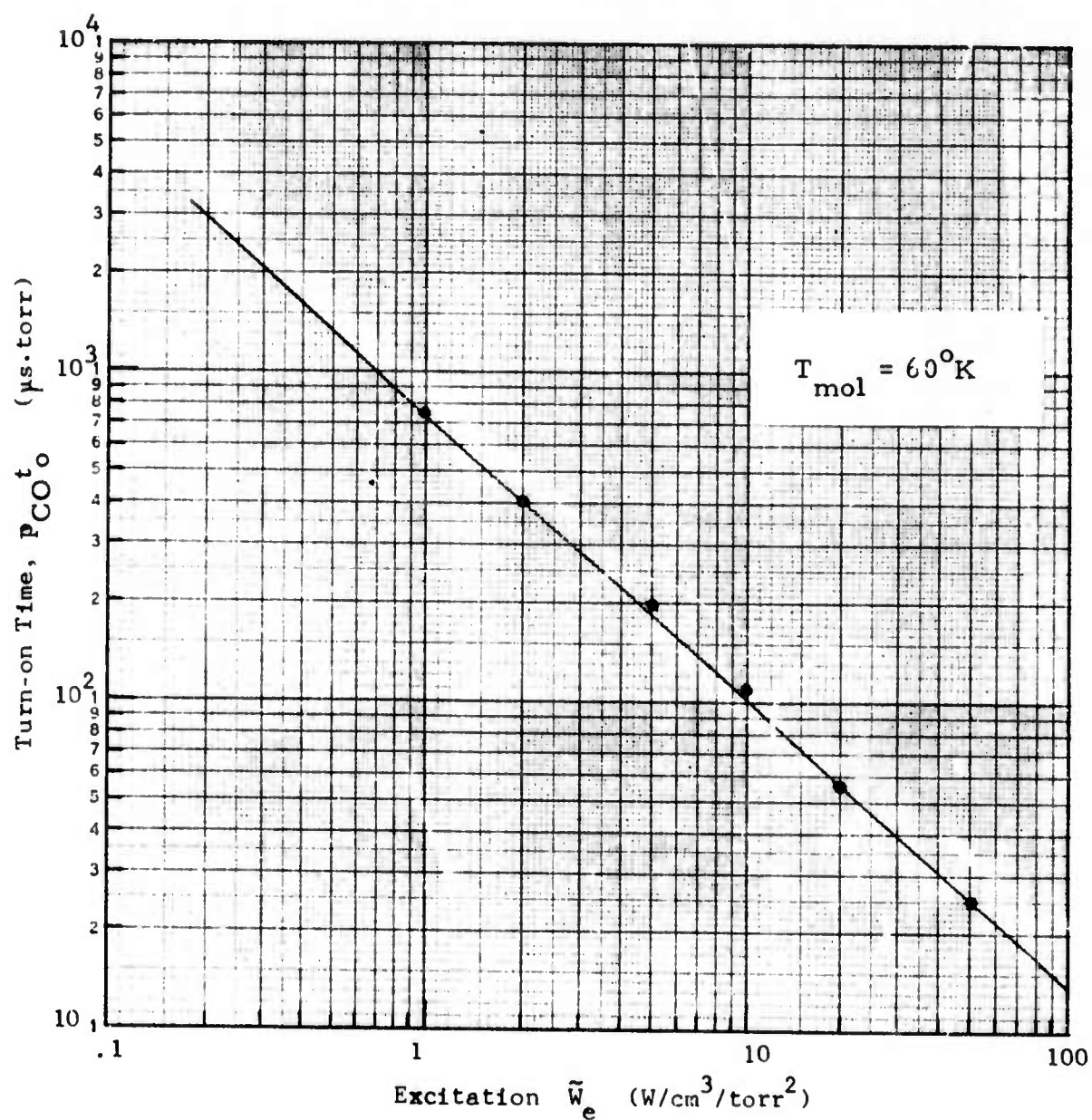


Figure 10. Scaled turn-on time as a function of scaled electrical pumping power.

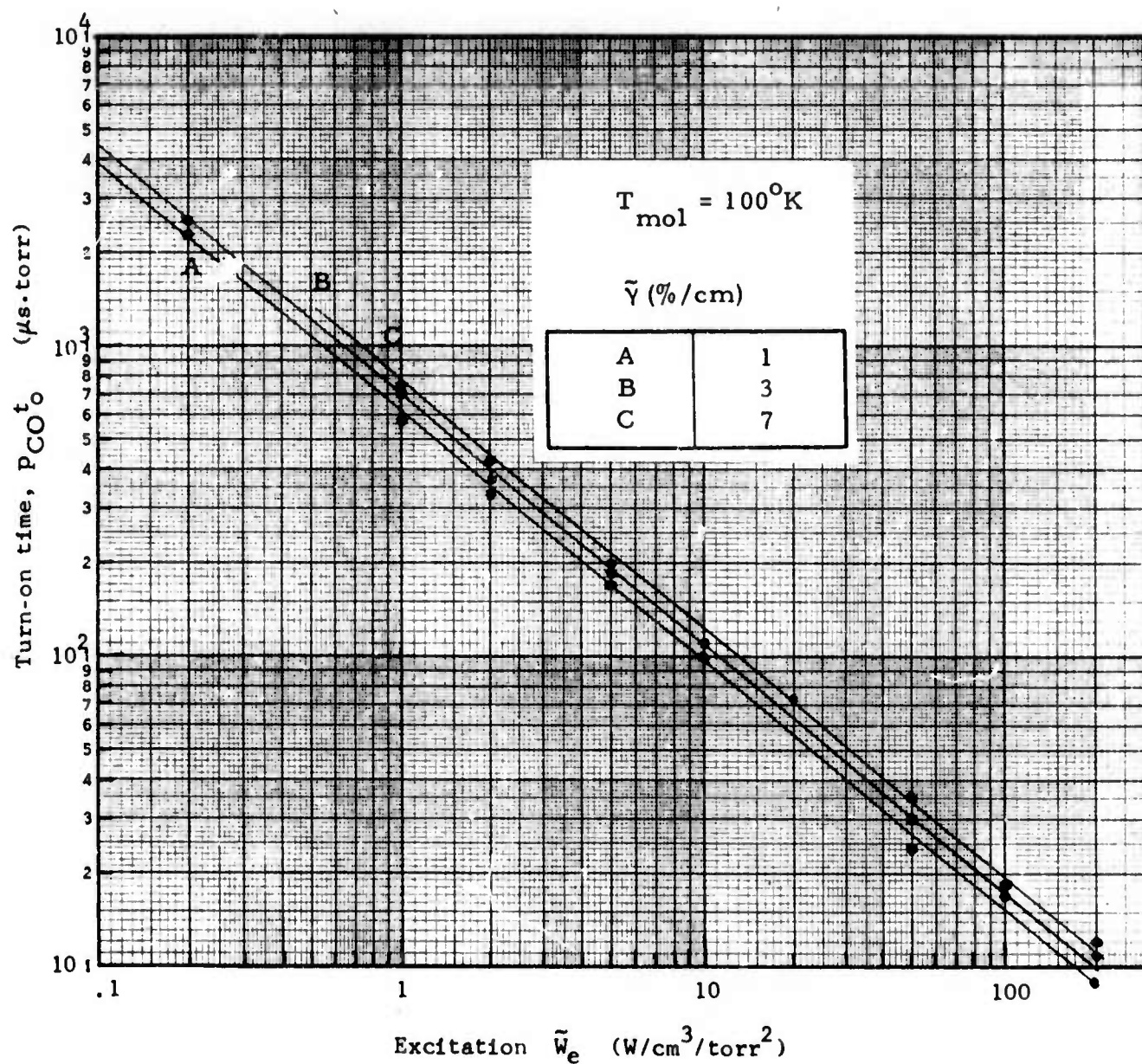


Figure 11. Scaled turn-on time as a function of scaled electrical pumping power.

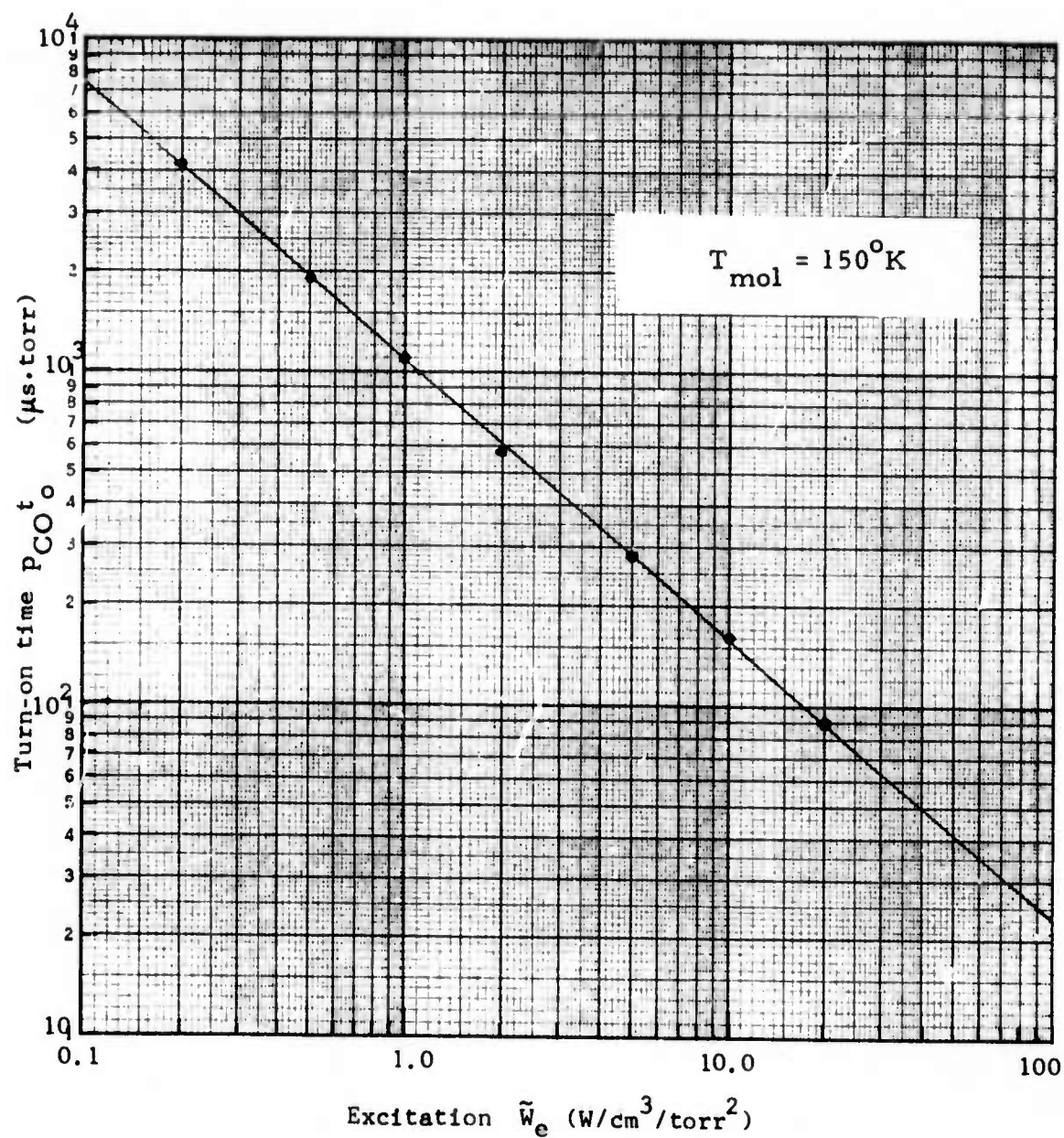


Figure 12. Scaled turn-on time as a function of scaled electrical pumping power.

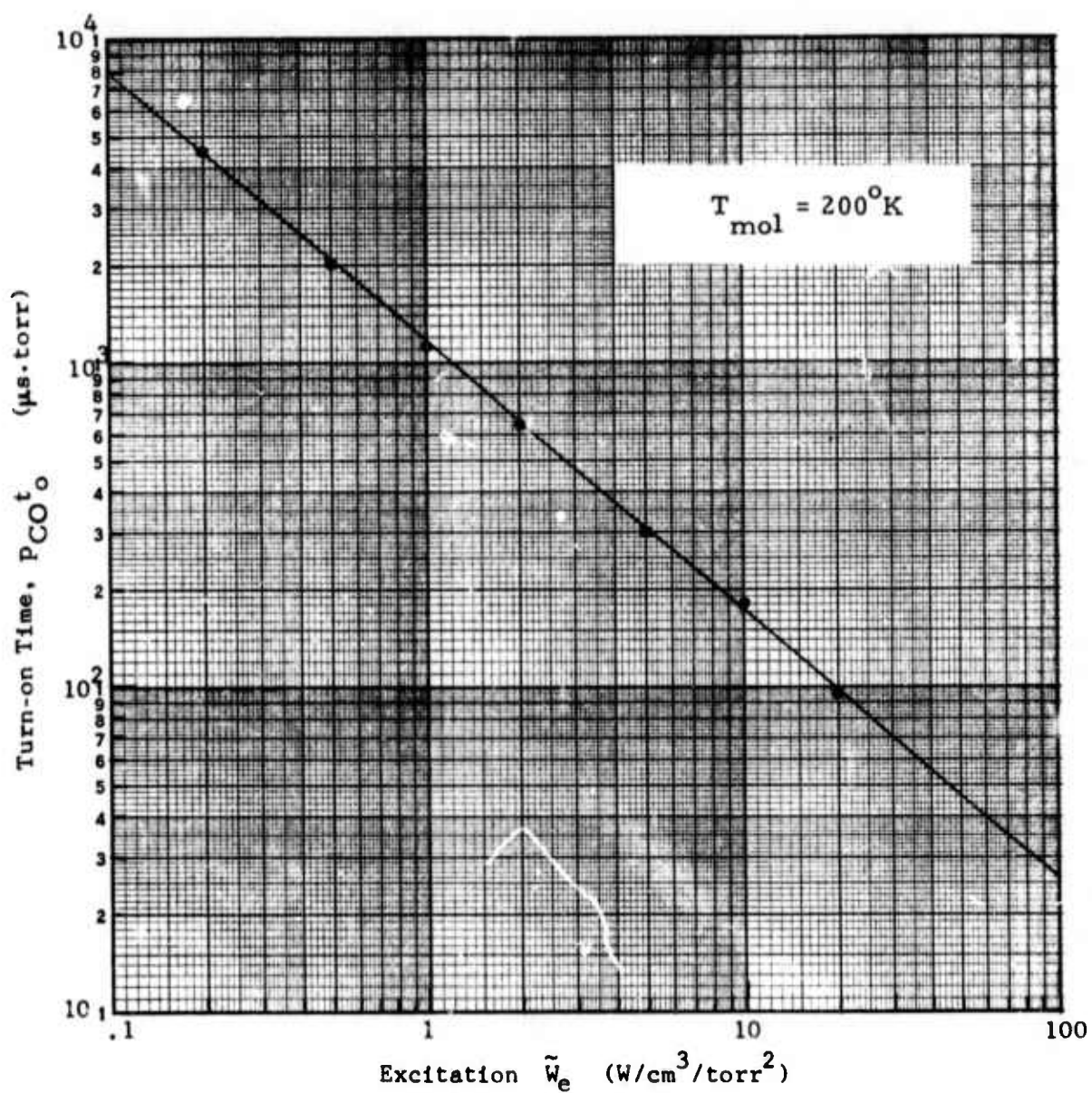


Figure 13. Scaled turn-on time as a function of scaled electrical pumping power.

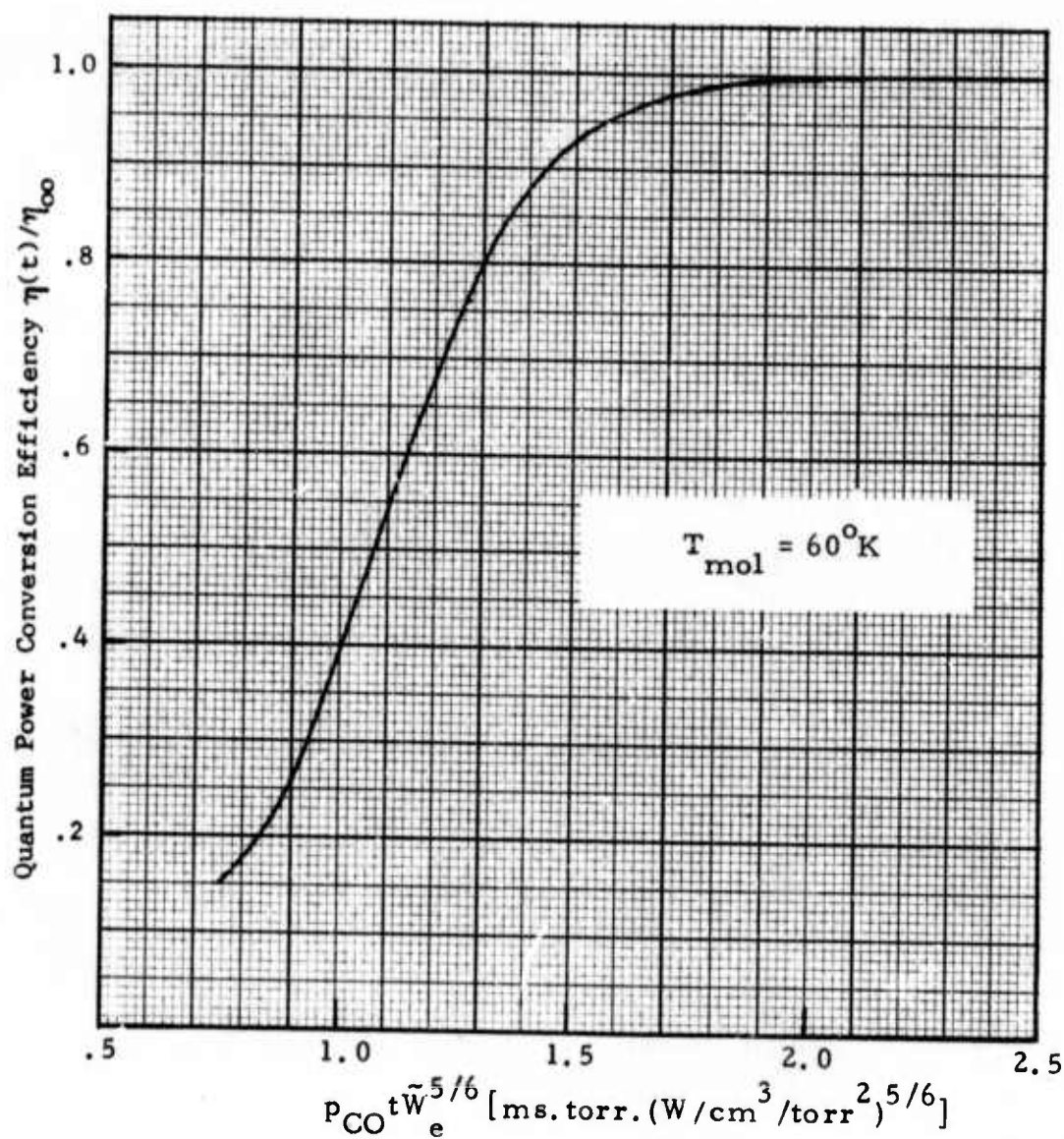


Figure 14. Quantum power efficiency as a function of the parameter $\tilde{e} = p_{\text{CO}} t_e^{5/6}$. Note that \tilde{e} is approximately energy deposited in units of J/liter/torr.

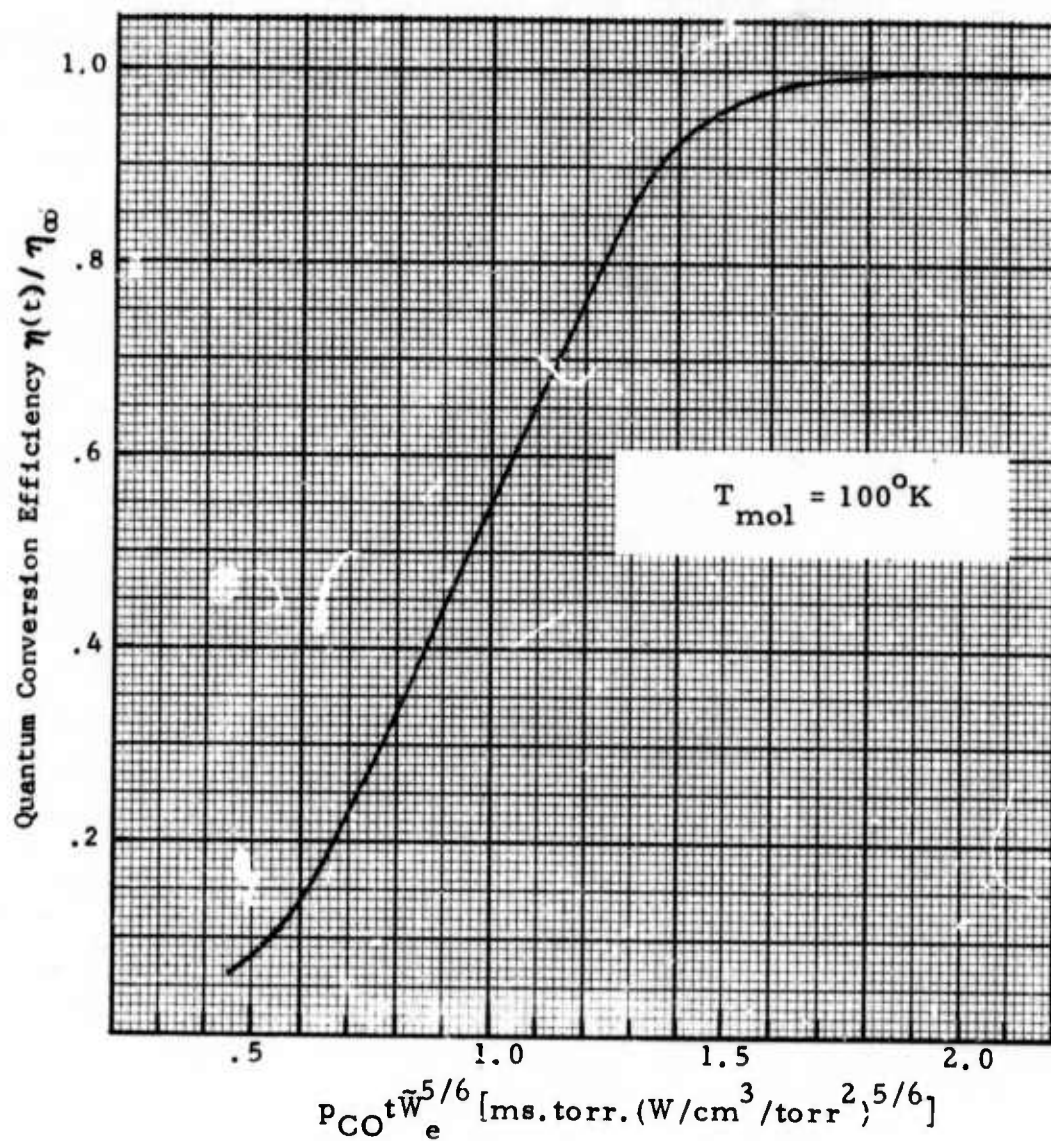


Figure 15. Quantum power efficiency as a function of parameter $\tilde{e} = p_{CO} t \tilde{W}_e^{5/6}$. Note that \tilde{e} is approximately energy deposited in units of J/liter/torr.

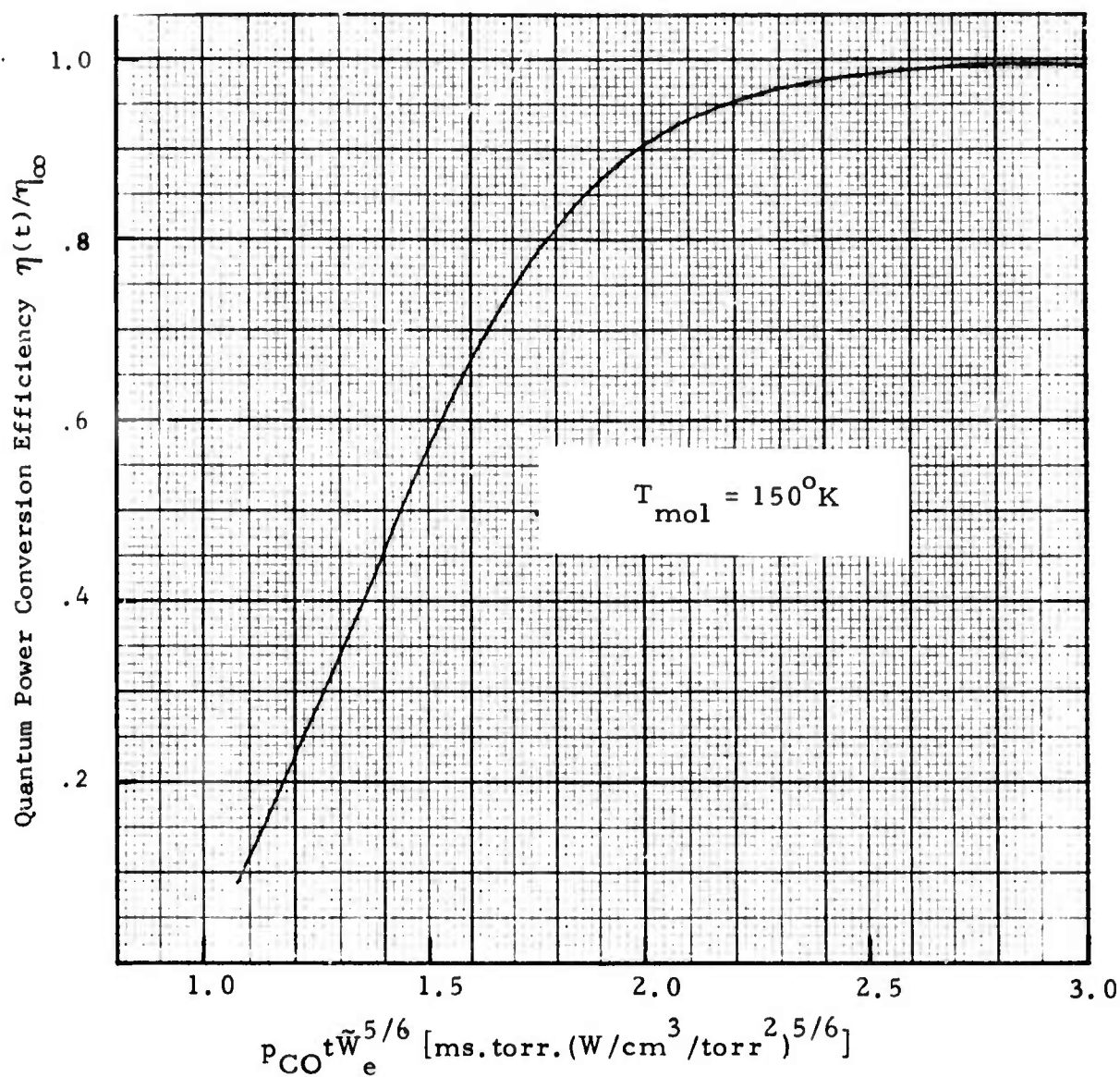


Figure 16. Quantum power efficiency as a function of parameter $\tilde{e} = p_{CO} t \tilde{W}_e^{5/6}$. Note that \tilde{e} is approximately energy deposited in units of J/liter/torr.

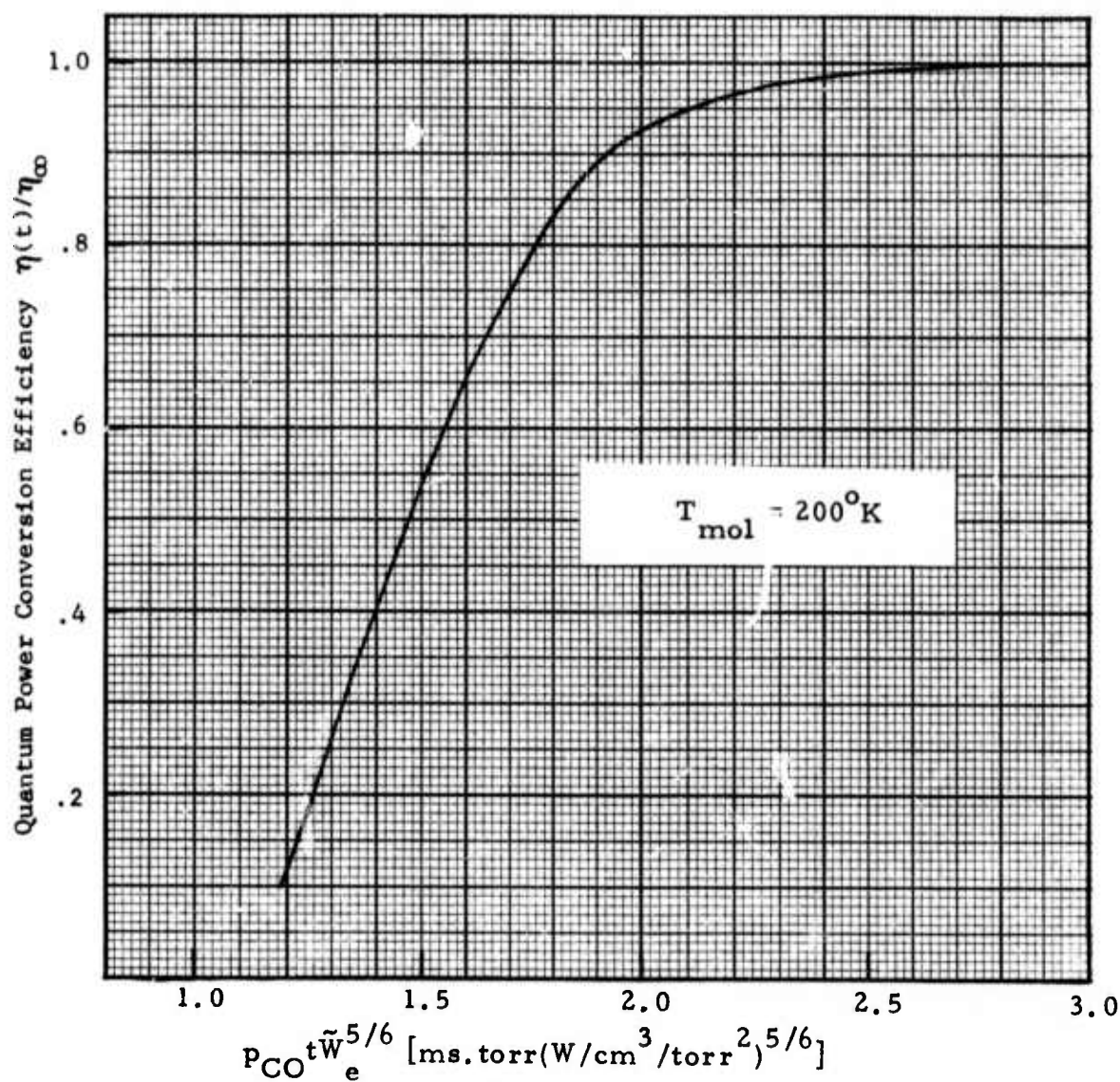


Figure 17. Quantum power efficiency as a function of parameter $\tilde{e} = p_{CO} t \tilde{W}_e^{5/6}$. Note that \tilde{e} is approximately energy deposited in units of J/liter/torr.

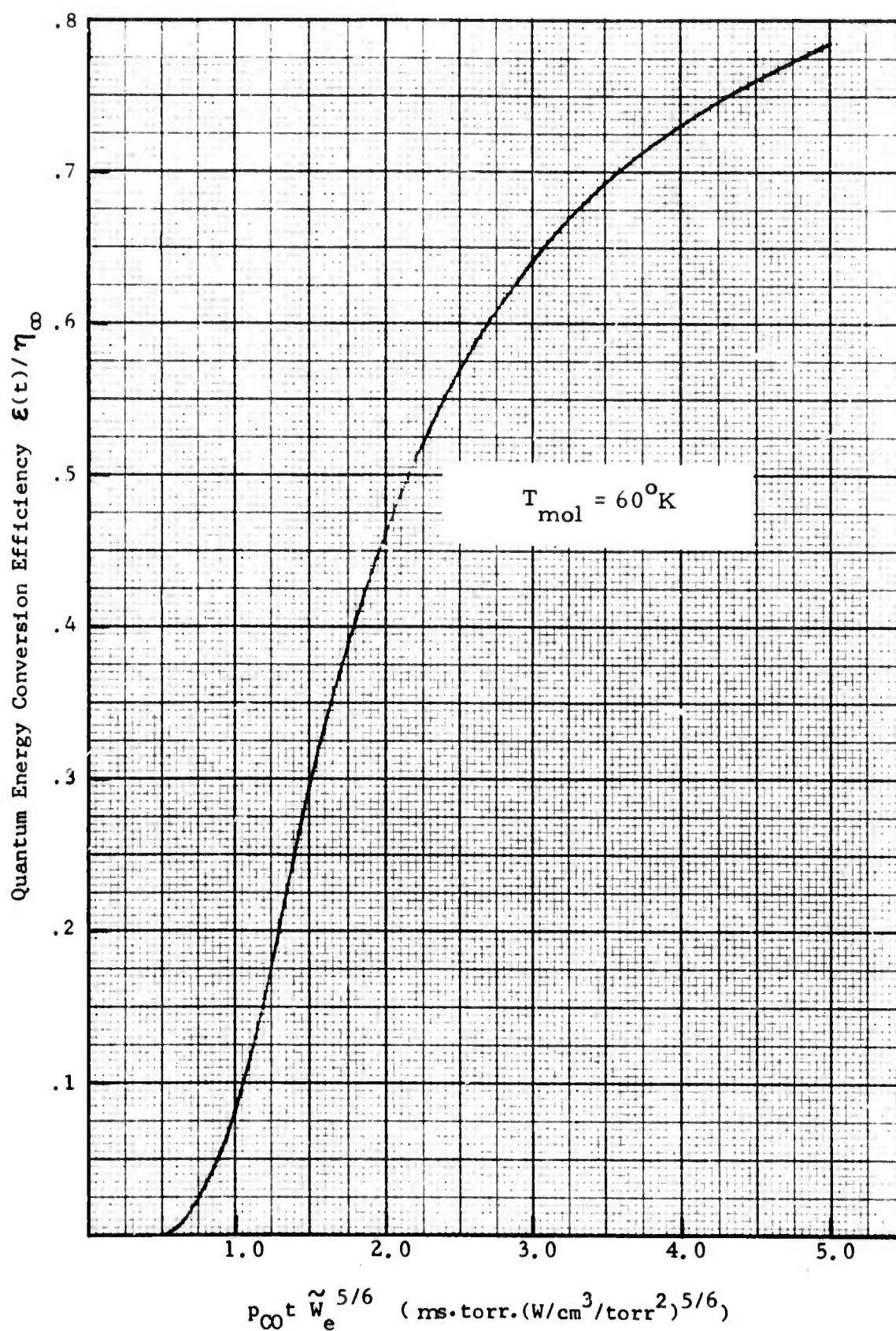


Figure 18. Quantum energy efficiency as a function of parameter $\tilde{e} = p_{CO} t \tilde{W}_e^{5/6}$. Note that \tilde{e} is approximately energy deposited in units of J/liter/torr.

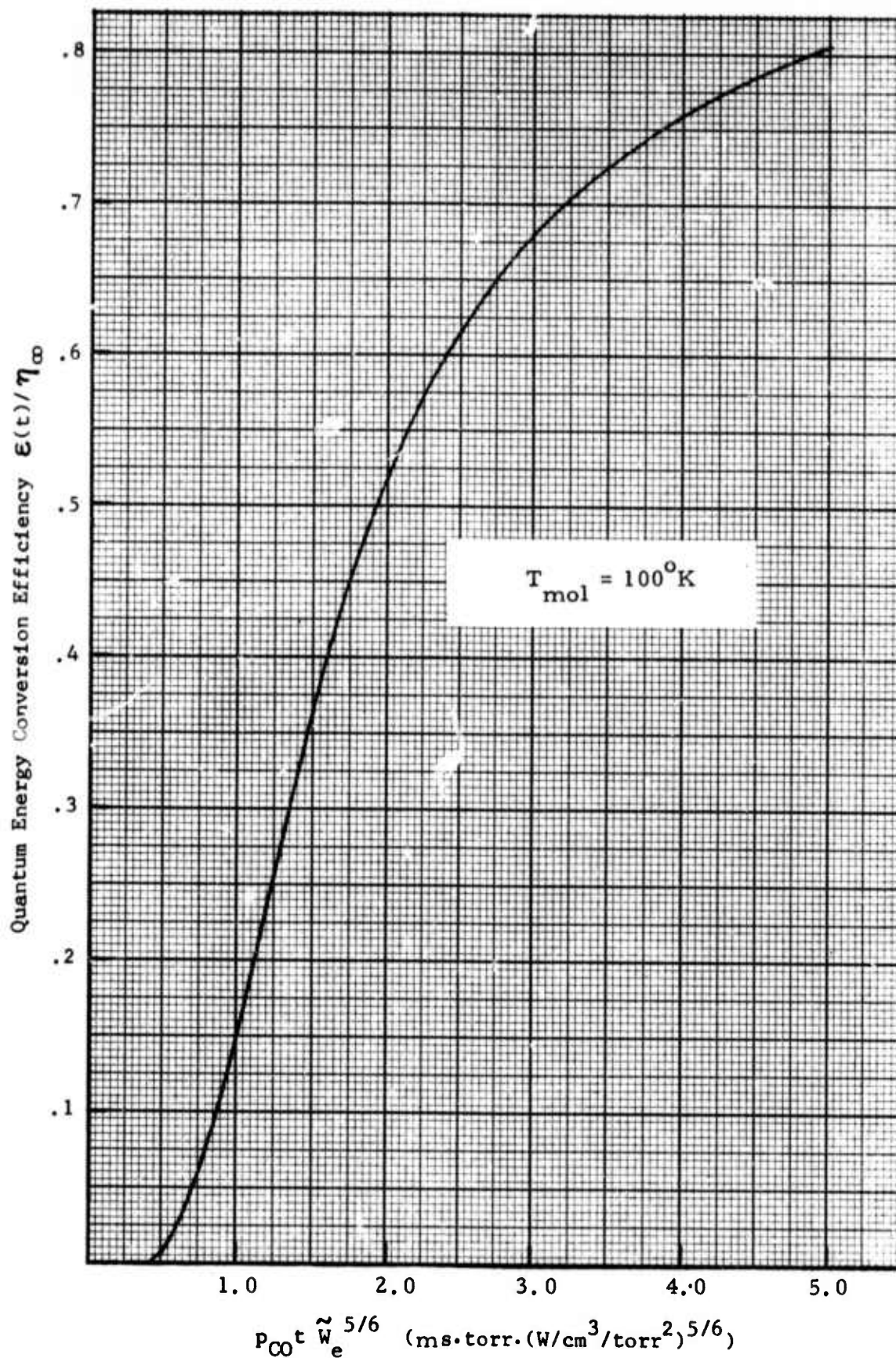


Figure 19. Quantum energy efficiency as a function of parameter $\tilde{e} = p_{\text{CO}} t \tilde{W}_e^{5/6}$. Note that \tilde{e} is approximately energy deposited in units of J/liter/torr.

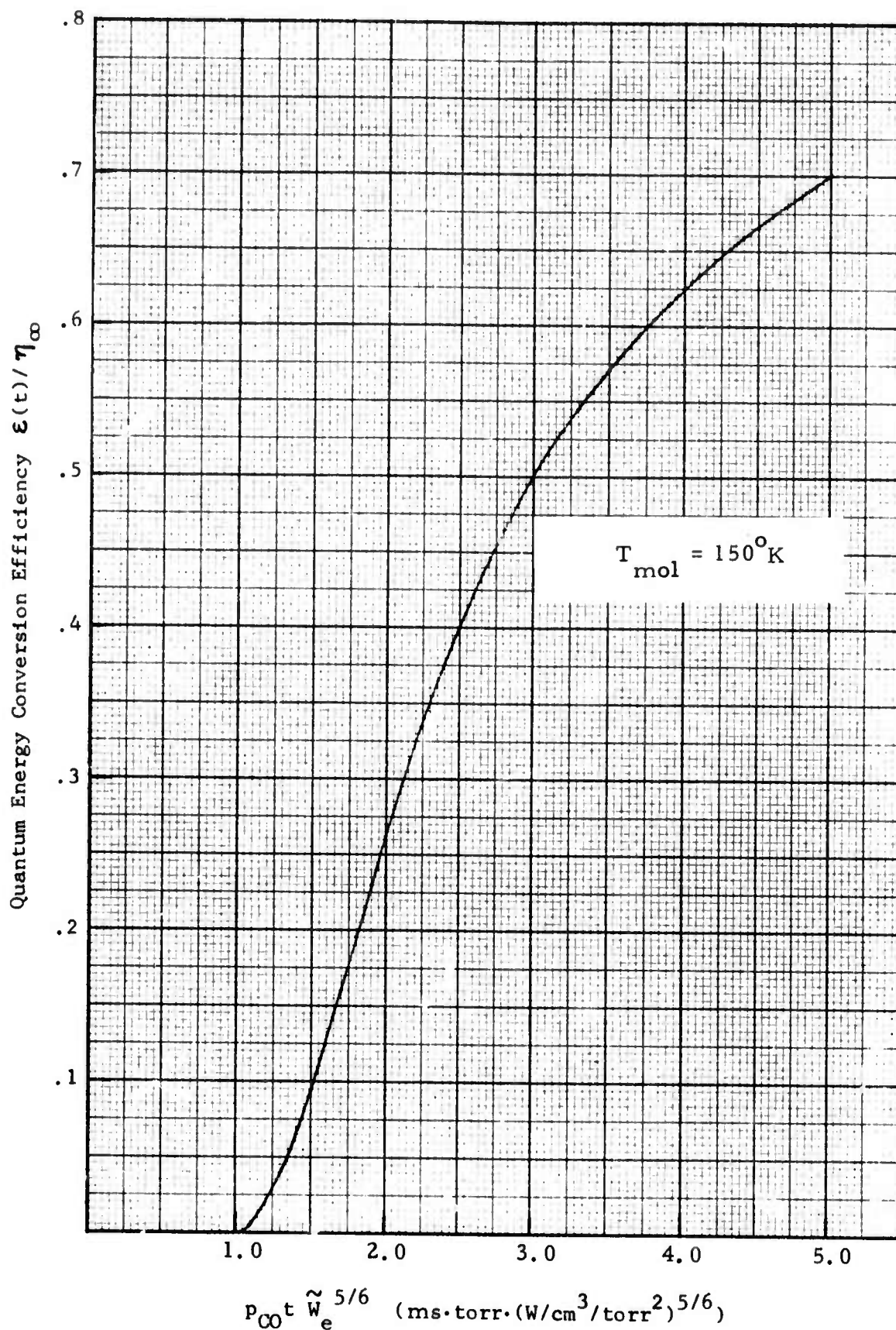


Figure 20. Quantum energy efficiency as a function of parameter $\tilde{e} = p_{CO} t \tilde{W}_e^{5/6}$. Note that \tilde{e} is approximately energy deposited in units of J/liter torr.

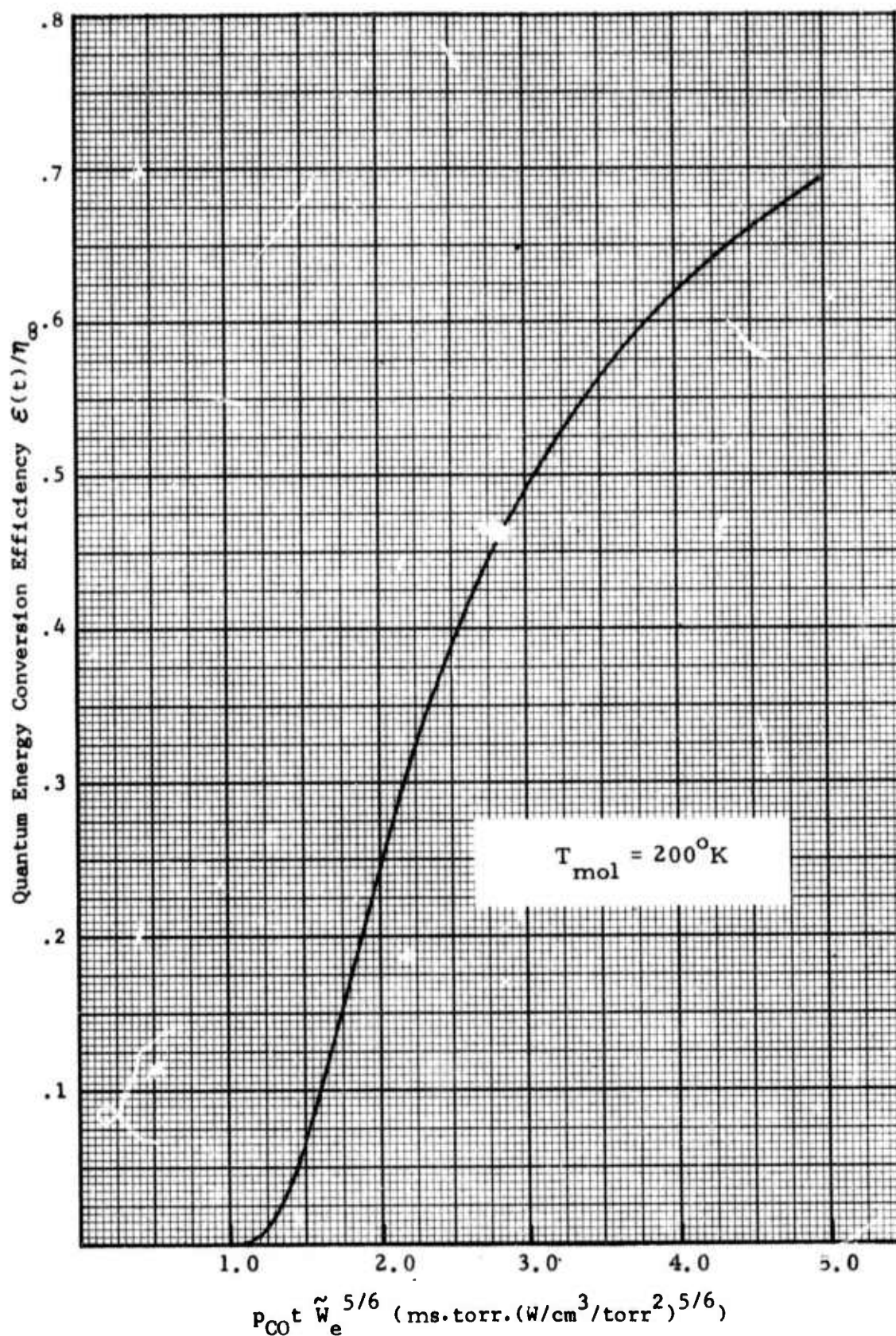


Figure 21. Quantum energy efficiency as a function of parameter $\tilde{e} = p_{CO} t \tilde{W}_e^{5/6}$. Note that \tilde{e} is approximately energy deposited in units of J/liter/torr.

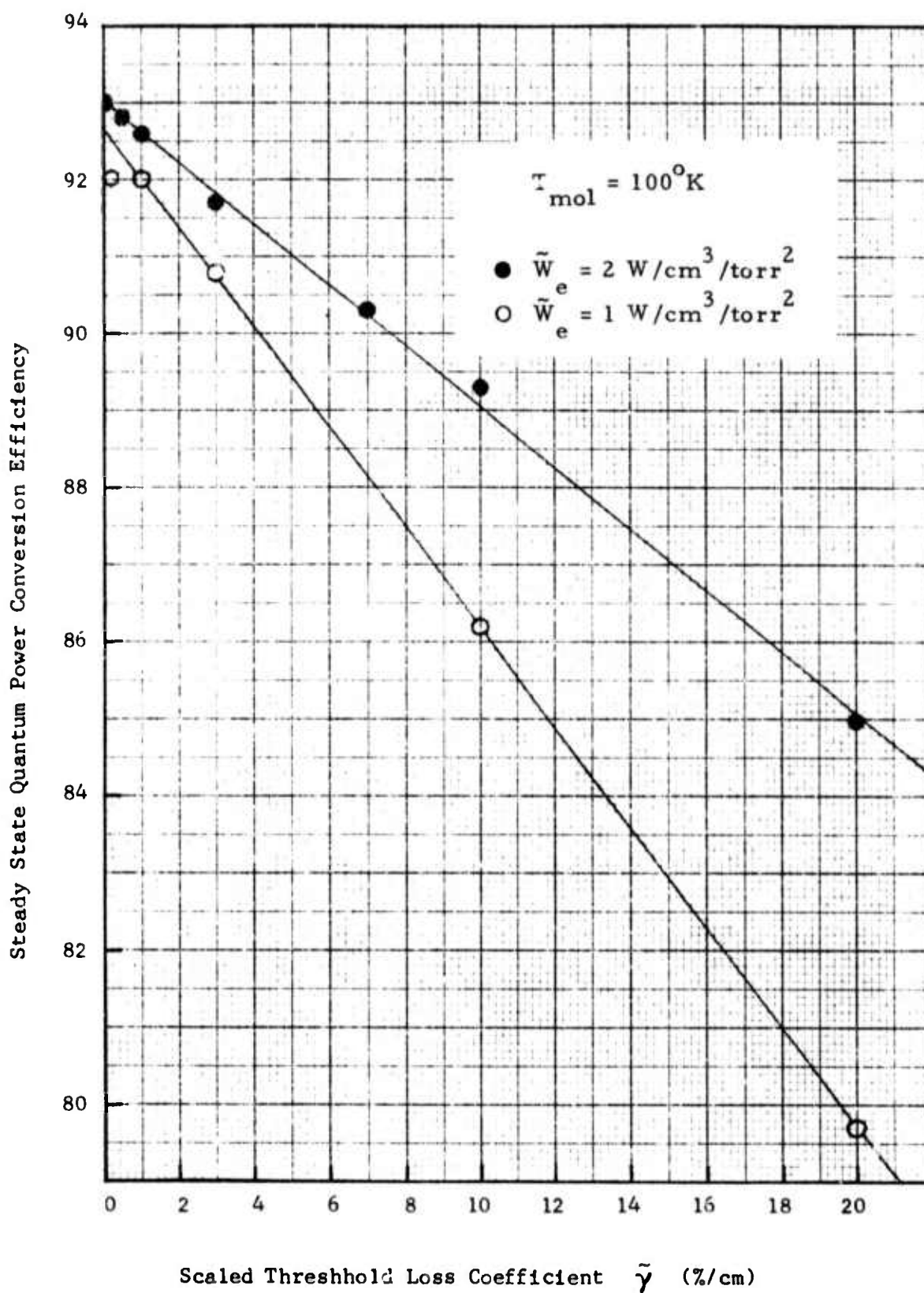


Figure 22. Saturation characteristics of a CO EDL after attainment of steady state; the slope of the curve is a measure of \tilde{W}_e/\tilde{I}_s .

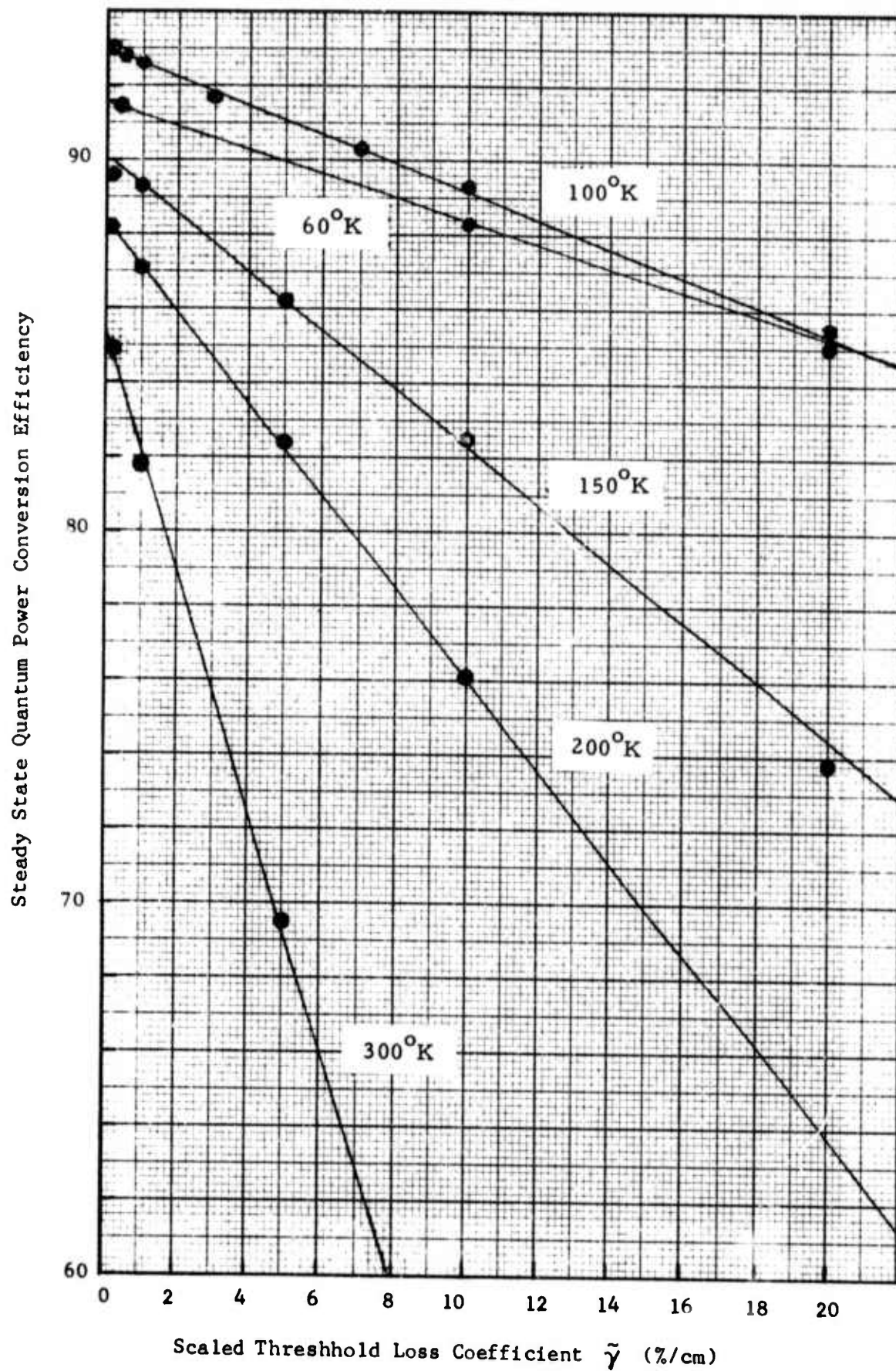


Figure 23. Saturation characteristics of a CO EDL after attainment of steady state; the slope of the curve is a measure of $\tilde{W}_e / \tilde{I}_s$.

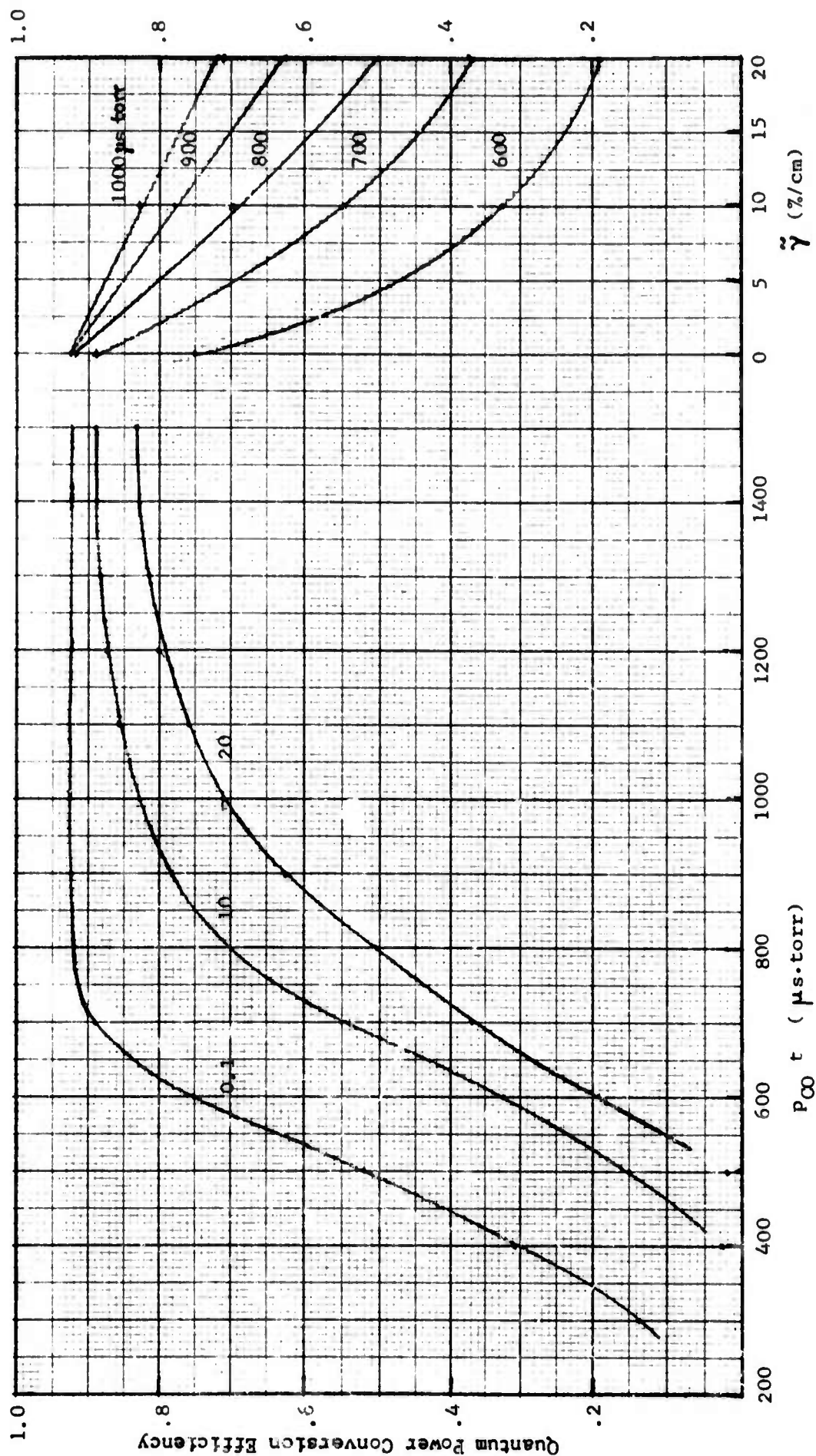


Figure 24. Saturation characteristics of a CO EDL investigated as a function of time. Curves on left are plots of quantum power efficiency $\eta(t)$ for three values of $\tilde{\gamma}$, and on right, $\eta(t)$ is plotted versus $\tilde{\gamma}$ for different values of $P_{CO} t$.

REFERENCES

1. W. B. Lacina, M. M. Mann, and G. L. McAllister, "Transient Oscillator Analysis of a High Pressure Electrically Excited CO Laser," IEEE Jour. Quant. Elect. QE-9, 588 (1973).
2. W. B. Lacina, "Kinetic Model and Theoretical Calculations for Steady State Analysis of an Electrically Excited CO Laser Amplifier System," Northrop Report NCL 71-32R, August 1971.
3. M. L. Bhaumik, W. B. Lacina, and M. M. Mann, "Vibrational Relaxation in CO Lasers," presented at Twenty Fifth Gaseous Electronics Conference, London, Ontario, Canada, October 1972.